Comparative Supramolecular Chemistry of Coronene and Hexahelicene: Helix Alignment in Crystalline Complexes with Trimesic Acid (= Benzene-1,3,5-tricarboxylic Acid) and π-Acceptor Compounds[1])

by **Otto Ermer*** and **Jörg Neudörfl**

Institut für Organische Chemie der Universität, Greinstrasse 4, D-50939 Köln

Dedicated to Professor *Edgar Heilbronner* on the occasion of his 80th birthday

The crystallization of the molecular complex $(TMA)_2 \cdot COR$ is reported, and evidence is produced that its structure is built up of planar hexagonal, H-bonded TMA honeycomb sheets, the large pores of which accommodate the almost perfectly complementary COR molecules by means of favorable straight C–H···O contacts. The detailed crystal structure of $(TMA)_2 \cdot COR$ could, however, not be unravelled by X-ray means, probably due to sheet stacking disorder. On the other hand, the crystals of the corresponding (racemic) complex $(TMA)_2 \cdot HEL$, engineered by exploiting the geometric similarities of HEL and COR, are fully ordered and have an analogous structure, although the HEL-filled TMA honeycomb sheets are puckered for improved 'helix following' *via* C–H···O contacts. The absence of stacking disorder is ascribed to the non-planarity of the HEL molecules protruding out of the mean plane of the TMA sheets. Further remarkable structural features of $(TMA)_2 \cdot HEL$ comprise: substantial helix flattening of HEL, perfect helix alignment (parallel helix axes of HEL molecules), TMA sheets with homochiral HEL guests, opposite chirality of HEL molecules in neighboring sheets, striking non-natural example of a mutually induced-fit molecular recognition process. In the ordered crystals of the racemic π donor-acceptor complexes HEL · TNB (two crystal forms), HEL · DNBA, HEL · TCNQ, and $(NIPA)_2 \cdot HEL$, the molecular helices of the HEL molecules are also well aligned, and, except for HEL · TNB, arranged in homochiral sheets. In these HEL sheets, some helix flattening is again observed, as well as head-to-tail contacts among the HEL molecules *via* protrusion into their molecular clefts. The crystal structure of $(NIPA)_2 \cdot HEL$ is particularly amazing and may be characterized as an elegant triply interpenetrating, distorted diamond architecture involving H-bonded NIPA zig-zag chains, which embrace the HEL molecules by means of C–H···O contacts with almost perfect 'helix following'. Simultaneously, good π donor-acceptor contacts between HEL and NIPA molecules are enabled, upon which the diamondoid model may also be based. Alternatively, the solid-state structure of $(NIPA)_2 \cdot HEL$ can also be viewed as a system of stacked, triply concatenated 'molecular fences' of the crossed lath-and-hinge type, with the laths representing the NIPA zig-zag chains and the HEL molecules providing the hinges. Both models account well for the alignment and chirality characteristics of the HEL sheets in $(NIPA)_2 \cdot HEL$. The crystal structure of the adduct PHEN · NIPA is also presented, which has architectural elements in common with $(NIPA)_2 \cdot HEL$, $(TMA)_2 \cdot HEL$, and $(TMA)_2 \cdot COR$. Apparently, PHEN · NIPA owes its stability in substantial measure to favorable C–H···O contacts ('C–H···O assisted π donor-acceptor complex'). Furthermore, the crystal architecture of PHEN · NIPA involves remarkably close intermolecular H···H contacts between neighboring PHEN molecules, which may be estimated as short as 1.86 Å, *i.e.*, more than 0.5 Å smaller than the *van der Waals* diameter of H. Finally, the crystal structures of the complexes COR · TNB and COR · DNBA are briefly reported and compared to the analogous HEL adducts. The COR molecules are twofold orientationally disordered in these molecular compounds, which involve the usual donor-acceptor π stacks, but with only limited alignment of the COR molecular disks. The complex $(NIPA)_2 \cdot COR$ could be crystallized, but resisted X-ray structure solution efforts, probably again due to substantial disorder phenomena. The corresponding pairs of COR and HEL molecular

[1]) Abbreviations of substances: COR, coronene; HEL, hexahelicene(= phenanthro[3,4-*c*]phenanthrene); ANN, [18]annulene (= cyclooctadeca-1,3,5,7,9,11,13,15,17-nonaene); PHEN, phenanthrene; ANTH, anthracene; TMA, trimesic acid (= benzene-1,3,5-tricarboxylic acid); PTA, pyridine-2,4,6-tricarboxylic acid; TNB, 1,3,5-trinitrobenzene; DNBA, 3,5-dinitrobenzoic acid; NIPA, 5-nitroisophthalic acid; TCNQ, 7,7,8,8-tetracyanoquinodimethane (= 2,2′-(cyclohexa-2,5-diene-1,4-diylidene)bis[propanedinitrile])

complexes studied generally agree in their stoichiometries, but differ conspicuously as regards their crystal-structural order, which is significantly perturbed if the perfectly circular, disk-shaped COR molecules are involved. The results are evaluated as regards the following prospects: recovery of COR from PAH mixtures, scanning-probe microscopic applications, extreme chiroptic and non-linear optical (NLO) properties of helix-aligned HEL molecular complexes, extension to crystalline adducts of other (higher) helicenes. Emphasis is laid on the stimulation of future attempts to engineer crystalline helix-aligned molecular complexes of optically active helicenes, which may be expected to bring forth particularly intriguing, useful, and extreme material properties.

1. Introduction. – This investigation grew out of a study of space-filling molecular models of coronene (COR) and trimesic acid (TMA; benzene-1,3,5-tricarboxylic acid) showing the virtually perfect complementarity of these molecules (*Fig. 1*), within the well-known H-bonded honeycomb sheets of TMA [1]. The COR molecules fit almost exactly into the hexagonal cavities of the planar super-graphite sheets of TMA, and the host-guest interactions appear attractive. Two symmetric orientations of the COR molecules inside the hexagonal holes of the TMA host sheets may be considered. The energetically preferable choice should correspond to *Fig. 1, a* rather than to *Fig. 1, b*, due to the better linearity of the 12 weak C–H···O H-bonds by which the COR guest molecules are anchored in the TMA host sheets. The highly symmetric overall pattern of good, almost linear C–H···O contacts of *Fig. 1, a*, clearly looks very suggestive and promising as regards the creation of a favorable TMA/COR 2:1 molecular complex of possibly even excellent stability.

2. Results and Discussion. – These expectations are fully born out by experiment. The TMA/COR 2:1 complex turned out to be practically insoluble in most organic solvents and may be precipitated instantaneously simply by pouring together solutions of TMA and COR (2:1 molar ratio) in suitable miscible solvents. An exception is provided by (hot) dimethylsulfoxide, which does dissolve the complex, probably supported by the fact that this solvent itself forms a rather stable complex with TMA [2a]. Obviously, the generally low solubility of $(TMA)_2 \cdot COR$ hints at substantial complex stability. Seemingly good and large deep-yellow crystals with the shape of slowly tapering needles or elongated bipyramids with hexagonal cross-sections could, *e.g.*, be obtained as follows: In a slim beaker, a COR solution in CS_2 is carefully covered by an 'insulating' layer of acetic acid, which in turn is covered by a solution of TMA in EtOH (1:2 molar ratio COR/TMA). After several days diffusion, crystals begin to appear at the glass walls, which may be harvested after growing for about two weeks. These shiny, transparent crystals may be cleaved extremely easily perpendicular to the hexagonal needle axis. Their lateral faces are not perfectly smooth but reveal, under the microscope, small growth steps (ripples) perpendicular to the needle axis. Towards polarized light, they are isotropic when viewed along the needle axis and sharply anisotropic perpendicular to it.

It is noted that the good complementarity of COR and the pores of the TMA honeycomb sheets has been seen previously, but this observation could not be put to good use since allegedly COR 'was poorly soluble in solvents useful for crystallizing trimesic acid' [1c]. As shown above, the key to the problem are diffusion methods applying different, yet miscible solvents with suitable polarities. For crystallization purposes, both COR and TMA are sufficiently soluble in CS_2/AcOH and $CHCl_3$/AcOH

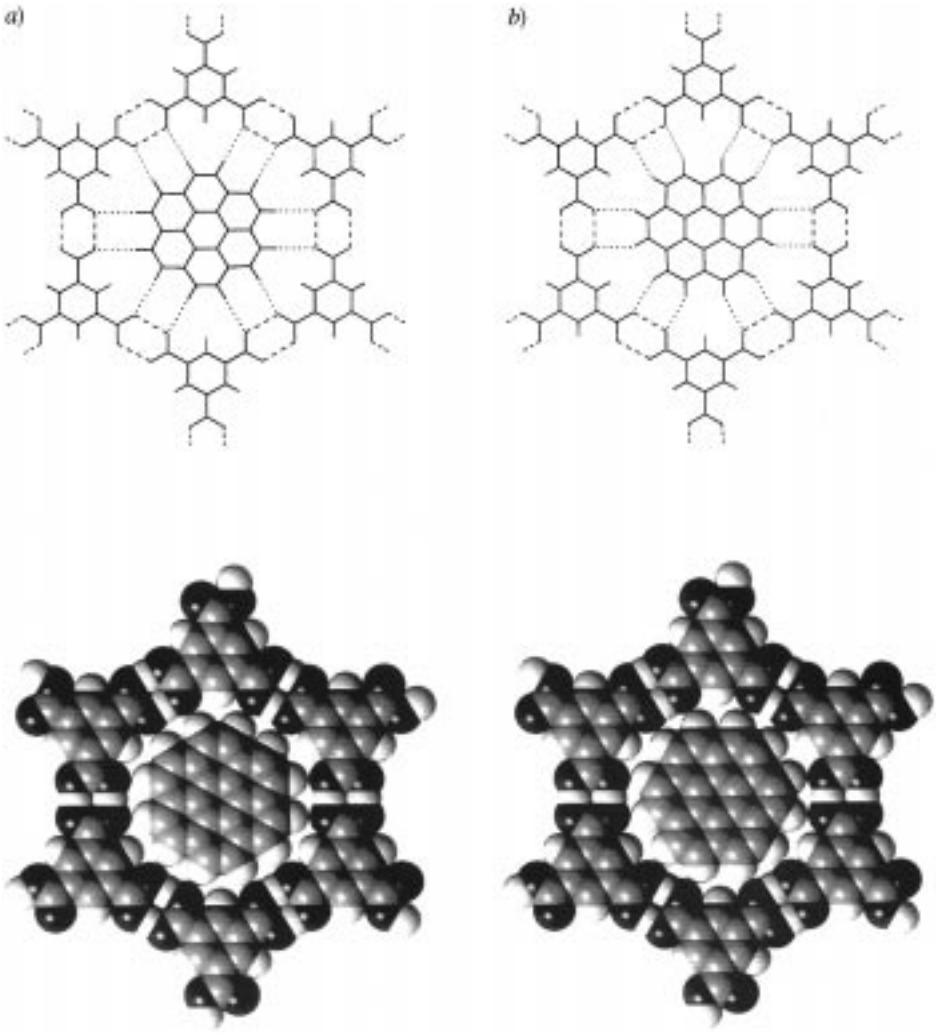

Fig. 1. *Suggested crystal structure of the molecular complex (TMA)$_2$·COR: section of the putative honeycomb-sheet architecture* a) *showing the probably preferred COR orientation with practically straight C–H···O contacts and* b) *the alternative symmetric COR orientation with less favorable, bent C–H···O contacts* (top: line drawings, bottom: space-filling representations). A hexagonal chamber cut out of a honeycomb sheet and formed by 6 doubly H-bonded (dashed) TMA molecules is shown, in which a COR guest molecule is anchored by means of C–H···O contacts (dotted). Both orientations of COR differ by a rotation of 30° around the molecular 6-fold axis. Note the perfect structural host-guest complementarity as highlighted by the space-filling drawings.

mixtures, *e.g.*, and this still holds for the respective ternary mixtures including EtOH. A molecular complex of TMA and pyrene together with EtOH could, however, be crystallized earlier [1c] and has structural features in common with those envisaged for (TMA)$_2$·COR (*Fig. 1*). The mutual orientation of the pyrene guest and TMA host

molecules is such as to support the architecture of *Fig. 1, a*, for $(TMA)_2 \cdot COR$, bearing in mind that the pyrene skeleton is a substructure of COR, of course.

All attempts to determine the structure by X-ray diffractometer measurements of variously grown $(TMA)_2 \cdot COR$ crystals failed. Heat treatment of the crystals (150° over 10 days) was tried, but did not help either. Similarly, numerous efforts to prepare crystalline molecular complexes of COR with other carboxylic acids related to TMA proved unrewarding. For example, suitable diffusion experiments with pyridine-2,4,6-tricarboxylic acid (PTA) gave orange-yellow hexagonal needles similar to those of $(TMA)_2 \cdot COR$, which, in particular, again showed extremely facile cleavage perpendicular to the needle axis. These crystals probably consist of the 2 : 1 molecular complex of PTA and COR, but no structural details could be obtained by X-ray diffraction, presumably due to disorder phenomena analogous to those in $(TMA)_2 \cdot COR$ as discussed subsequently[2]).

Precession photographs of the $(TMA)_2 \cdot COR$ crystals produced a reciprocal *hk*0 layer (perpendicular to the hexagonal needle axis) with reflections of good quality and

---

[2]) Triclinic crystals of a 2 : 2 : 1 molecular complex of PTA, H_2O, and AcOH could be grown and X-ray analyzed ($a = 8.4463(8)$, $b = 8.7402(9)$, $c = 16.1160(10)$ Å, $\alpha = 88.884(5)$, $\beta = 83.829(5)$, $\gamma = 66.953(3)°$, space group *P*-1, $Z = 4 + 4 + 2$, $R_1 = 0.059$, 2878 reflections), which are built up of porous $PTA \cdot H_2O$ sheets housing doubly H-bonded AcOH dimers in the cavities (see structure **A**). The involvement of the pyridine N-atoms in the H bonding is noteworthy. Sheet architectures with similar cavities have been encountered previously in crystalline hydrates of TMA [2b]. We also have preliminary X-ray evidence of a dihydrate of PTA with the N-atoms again involved in H bonding. Not unexpectedly, it would thus appear that the crystal chemistries of TMA and PTA are related although differences occur, which originate from the PTA N-atom striving to engage in H-bonding.

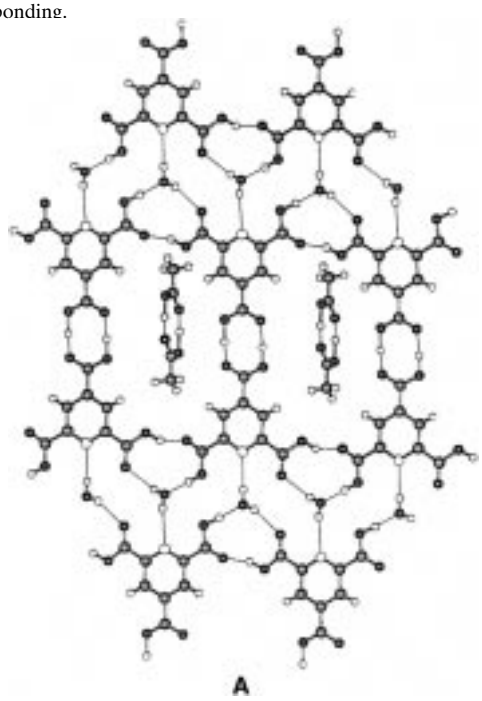

A

hexagonal symmetry from which the cell edges $a = b = 16.530$ Å could be derived. Layers perpendicular to *hk*0 show very few reflections with diffuse streaks extending along the hexagonal *c*-axis (needle axis). Particularly prominent is a highly intense axial 00l reflection corresponding to a spacing of 3.331 Å. These findings provide strong evidence in support of the planar hexagonal H-bonded super-graphite TMA sheets of *Fig. 1*, stacked at this very reasonable distance close to that of graphite itself (3.335 Å). The strong 00l reflection clearly owes its high intensity to in-phase scattering of all atoms in the planar layers without exception, similar to the very intense 002 reflection of normal (hexagonal) graphite. In crystalline COR itself, the interplanar spacing of the stacked molecules is somewhat larger (3.40 Å) [3], another hint at the propitiousness of the $(TMA)_2 \cdot COR$ complex. Apparently, the stacking of the planar honeycomb sheets is disordered thwarting the structure solution attempts. The distance of two doubly H-bonded TMA molecules is given by $a/\sqrt{3} = 16.530/\sqrt{3} = 9.544$ Å, from which an O···O separation of the H-bonds of 2.59 Å may be estimated, again in very good agreement with expectation. For both COR orientations of *Fig. 1*, an estimated value of 2.55 Å may be derived for the H···O distance of the C–H···O contacts. The corresponding C···O distance of the presumably more favorable orientation of *Fig. 1, a*, thus amounts to *ca.* 3.63 Å, perfectly in the normal range [4]. From the above X-ray spacings, a crystal density of 1.518 g cm^{-3} may be calculated, which compares favorably with the macroscopically measured value of 1.53 g cm^{-3} (flotation, CCl_4/$CHCl_3$). Conspicuously, the density of the $(TMA)_2 \cdot COR$ complex is higher than that of both components (TMA, 1.45 g cm^{-3} [1a]; COR, 1.39 g cm^{-3} [3]), once again attesting to its considerable stability.

Further non-crystallographic corroboration of the super-graphite structure of $(TMA)_2 \cdot COR$ comes from the following observations: The crystalline precipitate resulting from mixing TMA and COR solutions is homogeneous, and its 2:1 stoichiometry is confirmed by elemental analysis. The extremely facile cleavage of the crystals perpendicular to the hexagonal needle axis is in accord with a structure made up of weakly interacting sheets as in graphite itself. It should, therefore, lead to lubricant-like behavior of the $(TMA)_2 \cdot COR$ crystals, and this is indeed the case: When crushed between the fingers, the crystals feel soft and waxy similar to orthoboric acid, the H-bonded sheet structure of which [5] is even more closely related to $(TMA)_2 \cdot$ COR than that of graphite. Expectedly, however, the lubricant properties of graphite with its covalently bonded sheets are still more pronounced than those of the H-bonded congeners.

Summarizing all this evidence, it may be concluded almost beyond doubt that the molecular complex $(TMA)_2 \cdot COR$ builds up the anticipated planar hexagonal sheets in the crystal. Apart from the precise nature of the presumed stacking disorder of the sheets, the only essential piece of structural knowledge, which is left to be uncovered, concerns the orientation of the COR molecules in the hexagonal pores of the TMA host layers. As we have seen, there is reason to believe that the most favorable orientation corresponds to that shown in *Fig. 1, a*. Despite their circular disk shape, orientational disorder of the COR molecules (*via* rotation around the six-fold axis) within the TMA sheets appears unlikely, given the very favorable C–H···O contacts of *Fig. 1, a*, by which the hydrocarbon is suspended in the hexagonal host cavities. We deemed it worthwhile to carry our investigation one step further, and to try to reinforce

these latter suppositions by looking for TMA complexes with other aromatic hydrocarbons whose shape resembles that of COR. In this regard, [18]annulene (ANN) appears promising the outer rim of which is practically superimposable onto that of COR. However, ANN is not easy to prepare and chemically a rather sensitive material, and, still worse, one cannot reasonably hope for better prospects of avoiding a disordered stacking of the planar super-graphite sheets in the envisaged $(TMA)_2 \cdot ANN$ complex than in $(TMA)_2 \cdot COR$. Hexahelicene (HEL) is another aromatic hydrocarbon with a circumference similar to that of COR and ANN, and might thus serve as an enticing alternative in the present supramolecular context. Evidently, beyond its relation to $(TMA)_2 \cdot COR$, the targeted complex $(TMA)_2 \cdot HEL$ would constitute an intriguing structure in its own right, in particular in view of the helical chirality of HEL. HEL is a perfectly stable substance and may be easily handled at room temperature. However, HEL is severely nonplanar, of course, and a larger and more voluminous molecule than COR ($C_{26}H_{16}$ *vs.* $C_{24}H_{12}$), which might preclude a satisfactory stacking of the TMA honeycomb sheets filled with HEL molecules in the putative complex $(TMA)_2 \cdot HEL$. Nevertheless, we surmised the non-planarity of HEL might on the other hand constitute an advantage, since it could also lead to some helpful interdigitation of neighboring super-graphite sheets of the complex, thereby reducing the ease of gliding motions of the sheets perpendicular to the stacking axis. Viewed this way, the lateral HEL protrusions out of the plane of the hexagonal TMA host sheets may then be expected to reduce the danger of stacking disorder, which is what we want to engineer. As reported subsequently, these ideas indeed bore fruit, and a fully ordered 2 : 1 molecular complex of TMA and HEL could be created with structural attributes as envisaged and hoped-for.

The molecular complex $(TMA)_2 \cdot HEL$ was crystallized in the same way as $(TMA)_2 \cdot COR$ by covering in a large test tube a solution of racemic HEL in CS_2 by a layer of AcOH, and this in turn by a top layer of an ethanolic TMA solution (2 : 1 molar ratio TMA/HEL), and allowing for diffusion. This time, however, crystals grew only after subsequent slow evaporation of the solvent mixture, indicating enhanced solubility of the HEL complex and possibly lesser stability as compared to the $(TMA)_2 \cdot COR$ molecular compound. Once precipitated, however, the $(TMA)_2 \cdot HEL$ crystals do not easily redissolve. They take the shape of large pale-yellow, elongated six-sided prisms growing in individual groups, and may be cleaved with relative ease perpendicular to the long pseudo-hexagonal prism axes, although not as facile as the needles of the corresponding COR complex. These excellent single crystals were subjected to X-ray analysis, both at room and at low-temperature (105 K, see *Exper. Part* and the *Table*). Although the precision of the low temperature results is about twice as good as that of the room temperature data, mainly the latter are used in the following discussion for reasons of more meaningful comparisons with the crystal structures of HEL itself and a number of further HEL complexes to be described subsequently. A few low-temperature numerical data are nevertheless noted and clearly indicated as such. The crystals of $(TMA)_2 \cdot HEL$ adopt the centrosymmetric space group *C2*/*c*, with 8 molecules of TMA and 4 molecules of HEL in the unit cell. Thus the HEL molecules have crystallographic C_2 symmetry, yet the crystals as a whole are racemic. The density of the crystals is fairly high (calculated X-ray density 1.419, macroscopically measured 1.43 g cm^{-3}) as compared to HEL itself (1.280 g cm^{-3} [6]),

Table. *Crystal and Refinement Data*

	$(TMA)_2\cdot$ HEL		HEL· TNB	HEL· TNB	HEL· DNBA	HEL· TCNQ	$(NIPA)_2\cdot$ HEL	PHEN· NIPA
Crystal system	monoclinic		monoclinic	triclinic	monoclinic	monoclinic	monoclinic	triclinic
Space group	*C*2/*c*		$P2_1/c$	*P*-1	$P2_1$/c	$P2_1/c$	*Cc*	*P*-1
Z	4		4	4	4	8	12	4
T [K]	298	105	298	298	298	298	105	298
a [Å]	22.840(2)	23.0659(5)	8.0299(3)	8.1295(3)	7.7752(3)	8.2971(2)	13.2415(4)	7.2306(2)
b [Å]	16.209(2)	16.1783(4)	16.7514(5)	18.0448(5)	18.2049(5)	34.1708(5)	30.0686(7)	15.2513(5)
c [Å]	9.485(1)	9.1520(2)	18.9323(7)	18.0007(7)	18.6065(5)	19.6062(5)	25.8422(8)	16.5165(4)
α [°]				75.014(2)				90.700(2)
β [°]	93.599(5)	92.834(1)	98.582(1)	81.732(1)	101.444(1)	93.150(1)	102.555(1)	94.497(2)
γ [°]				86.523(2)				93.702(1)
V [Å^3]	3504.4	3411.1	2518.1	2523.5	2581.3	5550.3	10043.1	1811.7
d_x [g cm^{-3}]	1.419	1.458	1.428	1.425	1.391	1.275	1.489	1.427
d_m [g cm^{-3}][a]	1.43	–	–	–	–	–	1.46	–
N_{tot}[b]	6960	19912	23352	21043	25773	29417	27827	18790
N_{indep}[c]	3818	5183	5487	10882	4553	11980	14391	7880
N_{sig}[d]	2827	4805	3899	5999	2494	6617	10072	4823
ϱ_{res} [eÅ^{-3}][e]	0.16	0.40	0.17	0.19	0.13	0.27	0.55	0.17
R_{int}[f]	0.019	0.021	0.040	0.039	0.051	0.035	0.041	0.025
R_1[g]	0.042	0.043	0.045	0.054	0.049	0.052	0.070	0.051
wR_2[g]	0.111	0.117	0.112	0.140	0.140	0.152	0.208	0.146

[a]) The macroscopic densities d_m of $(TMA)_2\cdot$HEL and $(NIPA)_2\cdot$HEL were measured at room temperature by flotation in $CHCl_3$/benzene and H_2O/aq. KI solution, respectively. [b]) N_{tot}, total number of reflections recorded. [c]) N_{indep}, total number of independent reflections. [d]) N_{sig}, total number of significant independent reflections with $F>4\sigma(F)$. [e]) ϱ_{res}, maximum residual electron density. [f]) R_{int}, agreement index among intensities of equivalent reflections. [g]) R_1 and wR_2 indices include N_{sig} and N_{indep} reflections, respectively.

but somewhat lesser than that of TMA (1.45 g cm^{-3} [1a]), and smaller than that of $(TMA)_2\cdot$COR (1.518 g cm^{-3}, see above). This comparison suggests a rather good packing efficiency in the crystals of $(TMA)_2\cdot$HEL, although not as excellent as in $(TMA)_2\cdot$COR. Obviously, in view of the non-planarity of HEL, this could not reasonably have been expected any different.

The X-ray structure analysis of the crystals of $(TMA)_2\cdot$HEL shows that they are indeed built up of the characteristic hexagonal doubly H-bonded TMA honeycomb sheets with their large cavities housing the HEL guest molecules; *Figs. 2* and *3* provide stereo views of the architectural details of the sheets. Apart from the usual disorder of the H-positions in the carboxy H-bonds, this beautiful supramolecular fabric is fully ordered. Previous long-lasting efforts to engineer similarly structured TMA complexes, while successfully bringing about ordered super-graphite TMA host sheets, were not rewarded by equally ordered guest structures [1b]. A non-interpenetrating H-bonded honeycomb sheet structure has been successfully engineered by replacing the benzene H-atoms of TMA by butyl groups. The resulting tributyl-TMA does not take up guests, however, but fills the large hexagonal voids with its own butyl substituents [1c]. An expanded honeycomb sheet architecture related to that of TMA has been observed for the molecular complex $(TMA)_2\cdot$pyrene$\cdot(EtOH)_2$ mentioned above, the cavities of which are filled with pyrene and EtOH molecules [1c]. The orientation of the pyrene guest molecules relative to the TMA environment is analogous to that of HEL and (presumably) COR in the present complexes $(TMA)_2\cdot$HEL and $(TMA)_2\cdot$COR, respectively, as described below.

In the crystals of $(TMA)_2\cdot$HEL, the ordered structure of the HEL guest molecules in the TMA host cavities is apparently encouraged by the favorable C–H$\cdots$O contacts,

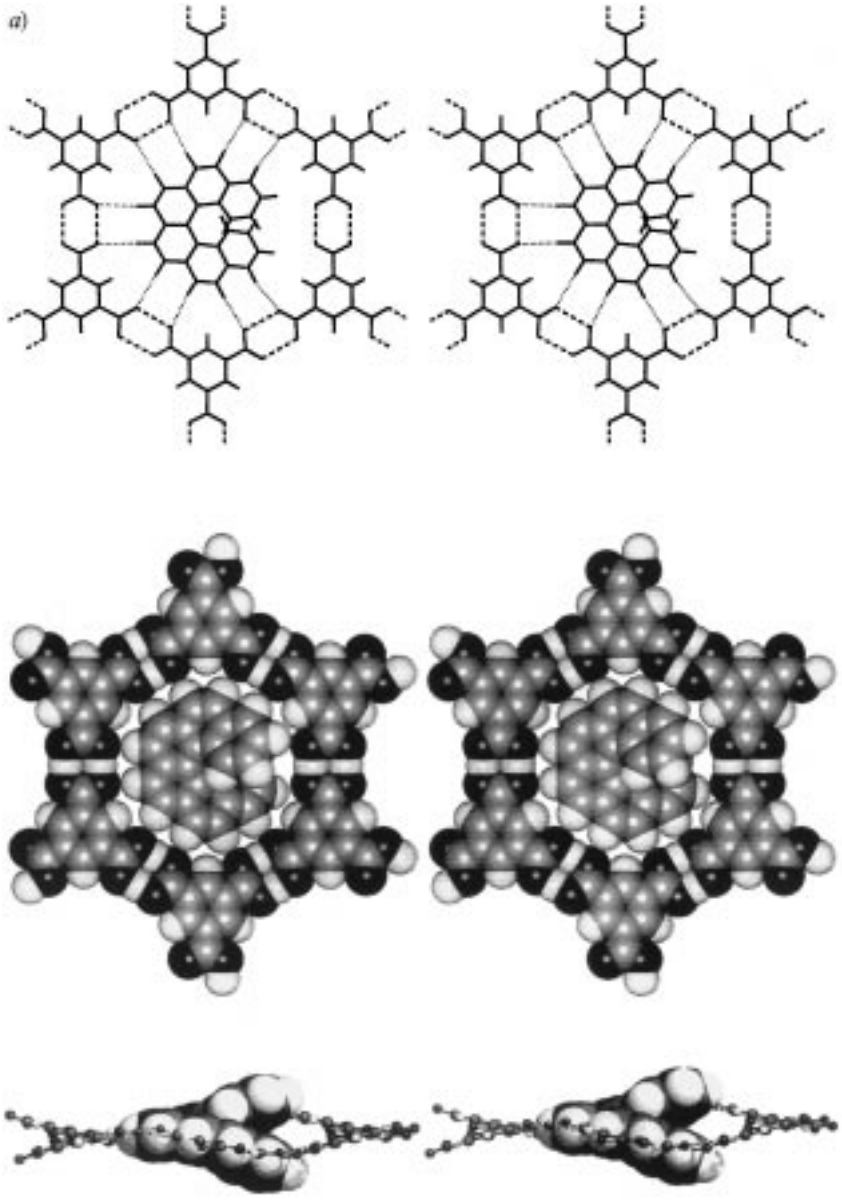

Fig. 2. a) *Stereoviews of the X-Ray crystal structure of (TMA)$_2$·HEL, with a HEL molecule suspended in a hexagonal TMA host chamber cut out of a honeycomb sheet.* Line diagram: O–H···O bonds dashed, C–H···O contacts dotted; space-filling drawing, with composite side view (bottom) illustrating the puckering of the TMA sheets; note the HEL orientation analogous to that expected for COR in (TMA)$_2$·COR, as shown in *Fig. 1, a*.

which can be established between guest and host molecules (*Figs. 2* and *3*). These weak C–H···O H-bonds mostly deviate only little from linearity despite the non-planarity of HEL (see below). Importantly in our context, it is evident from *Figs. 2* and *3* that the

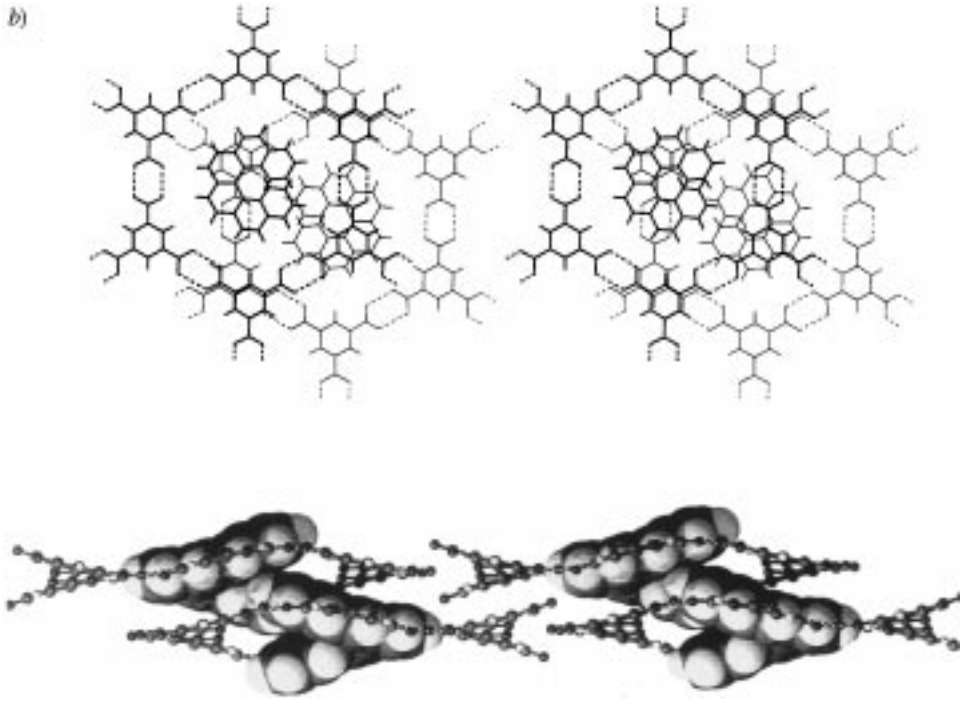

Fig. 2. b) *Similar line drawing as in* Fig. 2, a, *of two TMA chambers cut out of neighboring super-graphite sheets* (heavy and light lines, resp.) Bottom: composite side view; note the opposite chirality of the HEL guests.

orientation of the HEL molecules inside the TMA host cages is analogous to that shown in *Fig. 1, a*, and thus supports this orientational preference of COR in the $(TMA)_2 \cdot COR$ complex as supposed above. Still further support comes from the crystal architecture of the 1:1 molecular complex of phenanthrene and 5-nitroisophthalic acid to be described below (*vide infra, Fig. 10*).

The crystal structure of $(TMA)_2 \cdot HEL$ involves a number of intriguing features such that a description in some more detail seems justified. The H-bonded TMA host sheets are not planar but puckered in such a way that the carboxy O-atoms 'follow' the outer rim of the HEL guest molecules as effectively as possible, in order to attain good $C-H \cdots O$ contacts. This is achieved by moving the 4 O-atoms of the doubly H-bonded carboxy pairs, which in *Figs. 2, a* and *b*, and *3* run from left to right in zig-zag fashion, alternately above and below the mean plane of the TMA sheets by *ca.* 0.7 Å. This in turn is coupled with alternating tilts of the TMA molecules in opposite sense, brought about by rotations around axes, which run vertically in the mean plane of the sheets in *Figs. 2, a* and *b*, and *3*, and which protrude perpendicularly out of the drawing plane of the side views also shown in *Figs. 2, a* and *b*, and *3*. The molecular centers of the TMA molecules are essentially unaffected by these non-planar deformations and remain in the mean plane of the sheets. Lastly, small twisting deformations of the carboxy groups relative to the benzene rings of the TMA molecules as well as similar concomitant distortions of the doubly H-bonded carboxy pairs are observed, which also help to

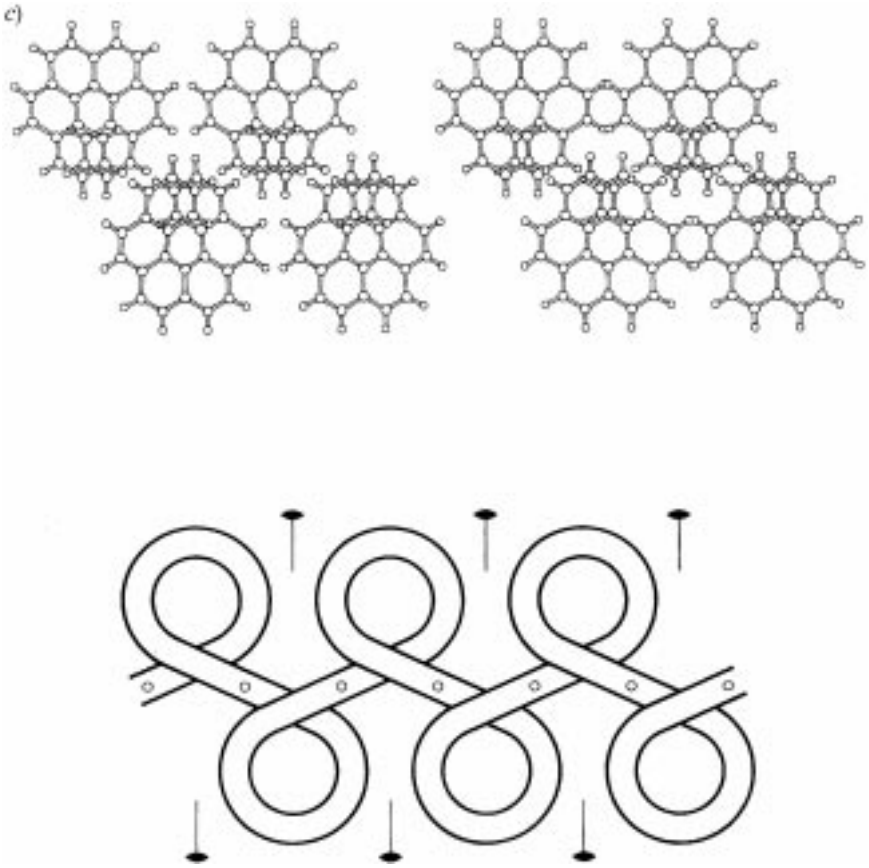

Fig. 2. c) *Sequence of helix-aligned HEL molecules belonging to consecutive supergraphite sheets of (TMA)$_2$·HEL* (top: the C_2-symmetric molecules have contact *via* their molecular clefts, and their chiralities alternate since they are related by crystallographic inversion centers) *and the diagrammatic representation of this achiral supramolecular pattern by the periodic ornament consisting of inverting figure-eight loops* (bottom: inversion centers (small circles) and twofold axes are indicated). The symmetry properties of the molecular pattern and the ornament are seen to fully agree.

improve the C–H···O contacts. As a consequence of the TMA tilts, the carboxy pairs running vertically in *Figs. 2, a* and *b*, and *3* move towards the inner cleft (or groove) of the HEL guests by *ca.* 0.3 Å, thereby improving the packing efficiency of the host-guest sheets. The puckering of the TMA sheets leads to a helical arrangement of the carboxy O-atoms surrounding the HEL molecules in the hexagonal cavities with like host and guest helicities. This 'helix following' of the TMA network enables 10 weak C–H···O H-bonds out of the 12 possible, *i.e.*, those analogous to COR, to assume geometries almost as favorable as in the (TMA)$_2$·COR complex with its entirely planar supergraphite sheets. (The 4 innermost H-atoms of the HEL molecules residing in the hexagonal TMA host cavities are not accessible for C–H···O bonding.) The C···O distances of the 10 close guest-host C–H···O contacts in (TMA)$_2$·HEL range from 3.535(2) to 3.651(2) Å (average 3.602 Å), and the C–H···O angles span values from

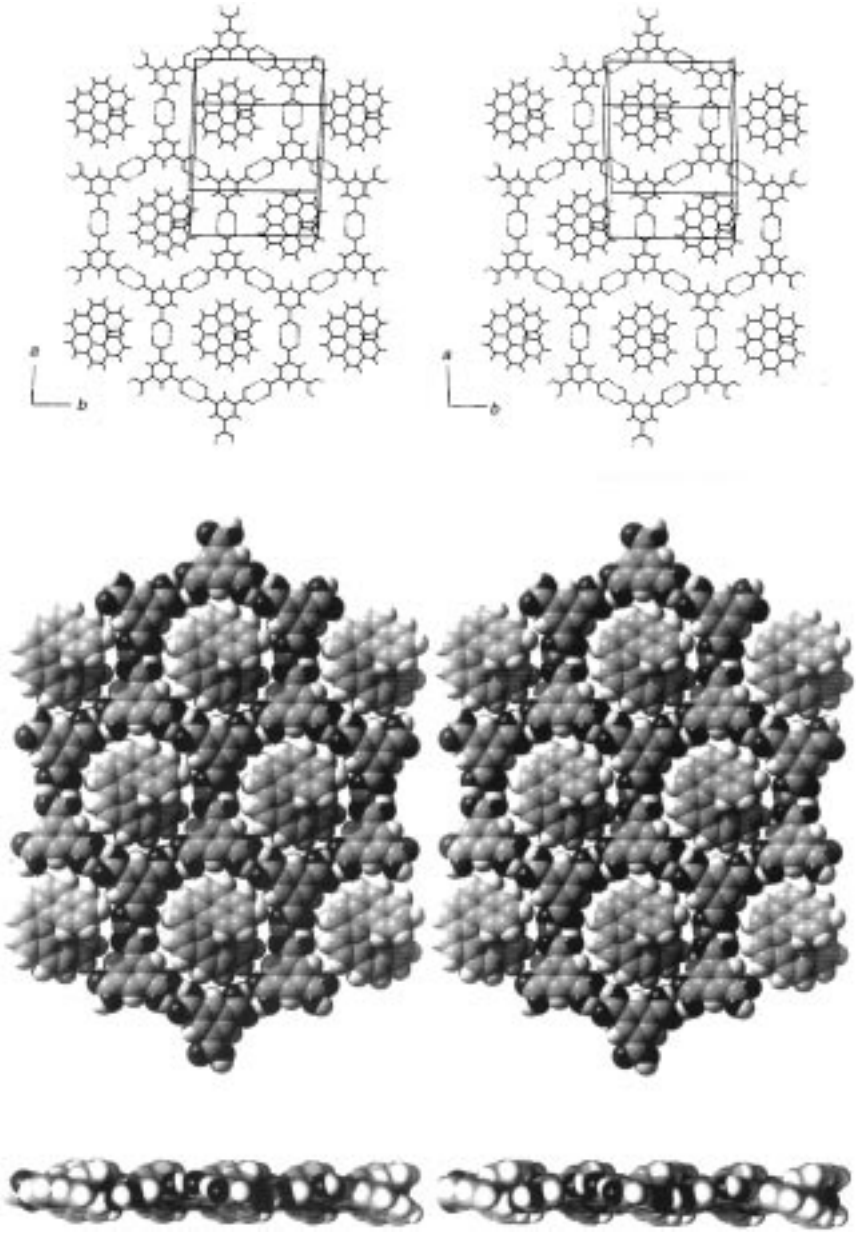

Fig. 3. *Section of a super-graphite honeycomb sheet of (TMA)$_2$·HEL* (stereoline (O–H···O bonds dashed) and space-filling drawings of top and side views). Note the homochirality and the alignment of the molecular helices of the HEL guests.

167(2) to 173(2)° (average 170°). At 105 K, the range of these C···O distances is from 3.498(1) to 3.622(1) Å (average 3.562 Å), and the C–H···O angles extend from 164(1) to 175(1)° (average 169°). The linearity of the C–H···O triads is thus seen to be rather

well established (*Fig. 2, a*). In addition to the good C–H···O contacts, the puckering of the TMA sheets, *i.e.*, in particular the TMA tilts, allow good π-contacts between TMA and HEL molecules belonging to neighboring sheets (*Fig. 2, b*). These contacts involve the 'wings' of the HEL molecules which, of course, are also tilted with respect to the mean plane of the sheets. The unexpectedly pronounced non-planar puckering deformations of the TMA sheets are not overly excessive, however, and do not lead to serious structural distortions of the doubly H-bonded carboxy pairs. Thus, the O···O distances of the O–H···O H-bonds take up normal values between 2.611(2) and 2.649(2) Å (average 2.632 Å; *Figs. 2* and *3*). Gratifyingly, all these non-bonded distances are thus seen to be similar to those estimated previously for the analogous complex $(TMA)_2 \cdot COR$ as described earlier (C···O 3.63, O···O 2.59 Å; see above). To put observations in perspective, it is noted that the honeycomb sheets of TMA itself are not planar either, but are severely pleated in order to allow effective cavity-filling *via* multiple self-interpenetration of the sheets [1a]. The sheet puckering modes in TMA and $(TMA)_2 \cdot HEL$ are entirely different, however. It would thus appear that quite generally non-planar distortions of the TMA honeycomb sheets are energetically not too costly.

The puckering of the super-graphite layers of $(TMA)_2 \cdot HEL$ oviously leads to recesses in the sheets, into which the branches of HEL molecules of neighboring sheets protrude. *Fig. 2, b* gives an idea of this interdigitation of the sheets in the complex and further shows that the contacts between the sheets are mainly brought about by face-to-face interactions between the π-systems of TMA and HEL molecules. The TMA host sheets are not stacked to form hexagonal channels but rather establish separate chambers in which the HEL guests reside. However, these chambers are still equipped with some sort of 'windows' through which the HEL wings protrude, thereby allowing contacts between HEL guest molecules of neighboring sheets whose chirality is opposite since they are related by crystallographic inversion centers (*Fig. 2, b*, see below). These guest-guest contacts may be described as an interdigitation of HEL grooves by means of interactions of inner H atoms with the π clouds of the neighboring molecule. The stacked TMA host sheets can be viewed to be threaded by chains of interdigitating HEL molecules with alternating chirality (*Fig. 2, c*), which may diagrammatically be represented by the ornament also shown in *Fig. 2, c*. This periodic motif consists of a sequence of inverting figure-eight loops and involves twofold rotation axes as well as inversion centers imposing achirality. An impressive enlarged section of this periodic frieze may be admired in the shape of the tracks of the Gotthard railroad near Faido, Tessin canton, Switzerland, running through a pair of tunnel loops of opposite helicity. Thus, since $(TMA)_2 \cdot HEL$ does not represent a channel inclusion compound, no face-to-face π contacts between neighboring HEL molecules are encountered. The stacking distance between the mean plane of the sheets in $(TMA)_2 \cdot$ HEL amounts to 3.759(2) Å (3.670(1) Å at 105 K), *ca.* 0.43° larger than in $(TMA)_2 \cdot$ COR. In view of the non-planarity of HEL, this is not surprising, but it is noted that due to the non-planar distortions of the TMA sheets in $(TMA)_2 \cdot HEL$ alluded to above, face-to-face π contacts within TMA-TMA and TMA-HEL pairs are enabled, which come close to those prevailing in $(TMA)_2 \cdot COR$.

It appears rather obvious that the stability of the complex $(TMA)_2 \cdot HEL$ should benefit from a flattening of the HEL molecule, since this would allow alleviated non-

planar distortions of the TMA host sheets as well. A closer look at the geometry of the complexed HEL molecule indeed reveals a very significant flattening as compared to uncomplexed HEL itself: The angle between the best planes of the two terminal six-membered benzene rings of HEL amounts to 42.0° (43.5° at 105 K) in the TMA complex as compared to 58.5° [6] in the crystals of HEL itself. Similarly, the non-bonded distance between the C-atoms of the two innermost methine groups is appreciably shortened upon complexation, *i.e.* from 3.227(3) to 2.944(2) Å. The flattening of HEL upon complexation with TMA is easily perceptible from the molecular drawings of *Figs. 4* and *5*. It thus appears that HEL is a relatively 'soft' molecule responding structurally to rather weak intermolecular forces. *Fig. 4* shows a superposition of the structures of TMA-complexed and uncomplexed HEL, together with the eigenvector (normal coordinate) of the lowest vibrational frequency of HEL as calculated by applying a modified consistent force field [7]. This frequency corresponds to a symmetric A mode and amounts to only 69 cm^{-1}. It may be seen from *Fig. 4* that the structural distortions of HEL upon complexation with TMA follow the normal coordinate of this soft vibrational mode in substantial measure. The force-field calculation thus confirms that the flattening of HEL is energetically not very demanding. The crystal structure of the complex $(TMA)_2 \cdot HEL$ provides an instructive non-natural example of the operation of the induced-fit principle, originally conceived to rationalize the mode of action of enzyme catalysis, that is the stability of enzyme · substrate complexes [8]. The induced fit in $(TMA)_2 \cdot HEL$ is indeed mutual and represents a particularly lucid case of a cooperative structural adaption of both the host and guest molecules, leading to improved complementarity: The non-planar puckering of the TMA sheets improves the guest-host C–H···O contacts, and the flattening of

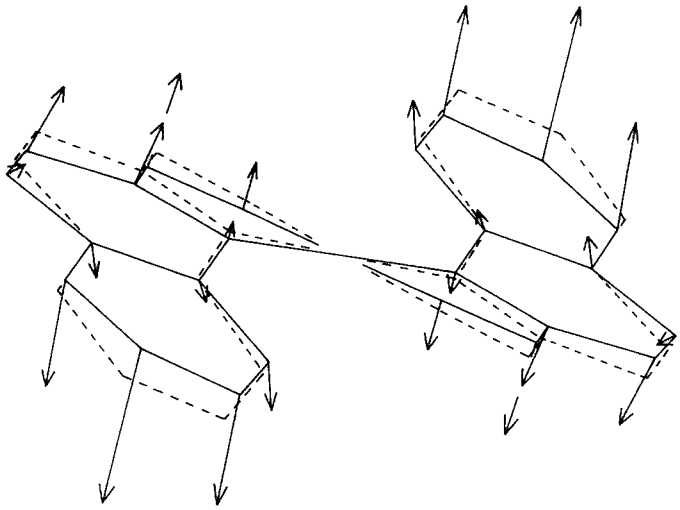

Fig. 4. *Flattening of HEL: superposition of the structures of HEL as observed in the crystals of* $(TMA)_2 \cdot HEL$ (solid) *and HEL itself* (dashed). Projection along the twofold molecular symmetry axes, H-atoms omitted. Attached to the atoms of the flattened HEL molecule are the atomic displacement vectors (scale arbitrary) of the normal coordinate of the calculated lowest vibrational frequency (69 cm^{-1}) of HEL. The components of these vectors perpendicular to the drawing plane are relatively small and not indicated.

HEL has this same effect and, in addition, allows better sheet stacking. Consequently, the cooperativity of the structural distortions of the complex partners, *i.e.*, TMA host puckering and HEL guest flattening, effects to keep them within acceptable limits. Of course, it is to be conceded finally that in principle the interplanar angle between the terminal benzene rings of HEL could be somewhat larger in its crystals than in gaseous HEL, due to some packing forces which may not obviously be assessed. Accordingly, the flattening of HEL in the crystals of $(TMA)_2 \cdot HEL$ would in this case have to be judged a little less extreme.

Fig. 5 provides a pictorial comparison of the anisotropic temperature motion of the HEL C-atoms in $(TMA)_2 \cdot HEL$ and free HEL. The comparatively large atomic displacements in free HEL are conspicuous, especially in the outer rim away from the molecular cleft. More quantitatively, the equivalent isotropic temperature factors U_{eq} of HEL in $(TMA)_2 \cdot HEL$ are from 4 to 17% smaller than in free HEL (average 12%, *i.e.* $\langle U_{eq} \rangle = 0.0731$ *vs.* 0.0827 Å^2; room temperature), whereas the corresponding relative differences of the largest anisotropic eigenvalues U_1° even range from 7 to 39% smaller in the complex (average 25%, *i.e.*, $\langle U_1^\circ \rangle = 0.1017$ vs. 0.1361 Å^2). Shape and directionality of the vibrational ellipsoids of *Fig. 5* are very suggestive as to hold the guest-host C–H···O contacts in $(TMA)_2 \cdot HEL$ responsible for these differences, which give rise to a relatively tight anchoring of the HEL molecules in the TMA host voids. This should mainly lead to a reduced librational molecular motion approximately around the helical axis, and that is essentially what may be gleaned qualitatively from the vibrational ellipsoid plots. A more quantitative computational effort would be required to account for other details of the thermal motion differences of the HEL molecules in the two different molecular environments. It is noted that at 105 K, the averages $\langle U_{eq} \rangle$ and $\langle U_1^\circ \rangle$ of the HEL C-atoms in $(TMA)_2 \cdot HEL$ assume the values 0.0297 and 0.0418 Å, respectively (reduction to 41% of room-temperature values).

One important aspect of the crystal structure of $(TMA)_2 \cdot HEL$ remains to be discussed, which hinges upon chirality and helicity of HEL. As dictated by the centrosymmetric space group, *C*2/*c*, and in view of the racemic sample used for the crystallizations (*cf.* above and *Exper. Part*), the crystal structure of $(TMA)_2 \cdot HEL$ as a whole is achiral. However, the individual super-graphite sheets building up the 3D crystal architecture are chiral. This means that the chirality of all HEL molecules housed by one particular TMA host sheet is the same (homochirality, *Fig. 3*). HEL molecules of neighboring $(TMA)_2 \cdot HEL$ layers have opposite chirality, such that the complete solid-state structure consists of stacked super-graphite sheets of alternating chirality. In terms of crystal symmetry, molecules of neighboring sheets are accordingly related by inversion centers and glide planes, whereas molecules within one and the same sheet are connected *via* translations, twofold rotation axes, and twofold screw axes. Since the crystallizations were performed with racemic HEL, that is by offering both enantiomers to the TMA host molecules, it would appear that the observed stacking of host-guest sheets with alternating chirality is energetically preferred over a stacking of sheets of like chirality. It is, however, difficult to estimate to what extent the stacking of $(TMA)_2 \cdot HEL$ honeycomb sheets of like chirality is impaired, and whether this stacking could, *e.g.*, only be accomplished at the expense of creating intolerably large empty spaces rendering a crystalline $(TMA)_2 \cdot HEL$ complex with nonracemic, enantiomerically pure HEL unstable. This important point is again discussed in *Sect. 3*.

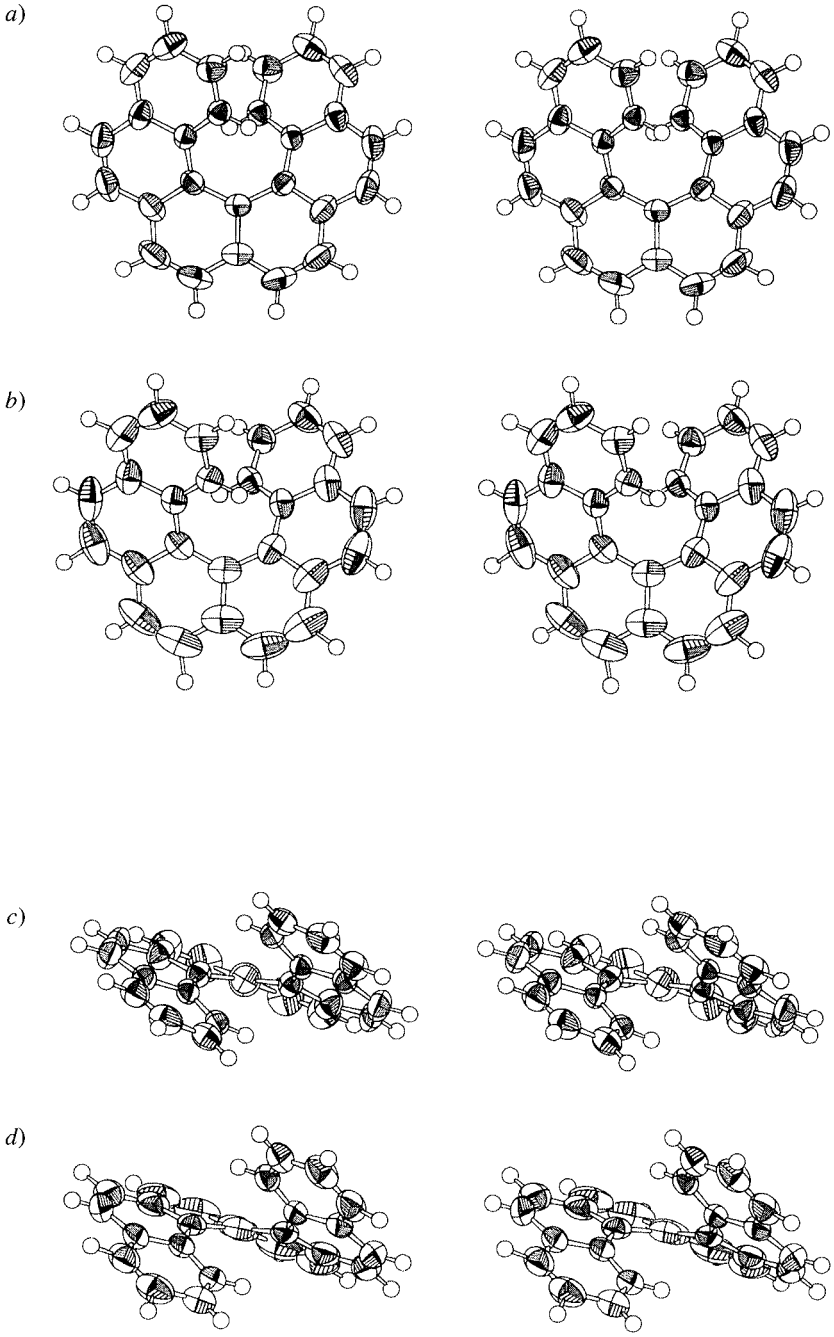

Fig. 5. *Temperature motion of HEL: stereoviews basically* a) b) *along the helix axis and* c) d) *along the twofold axis of the HEL molecule with 50% vibrational ellipsoids, observed at room temperature in the crystals of* a) c) $(TMA)_2 \cdot HEL$ *and* b) d) *HEL itself.* The H-atoms are represented by spheres of arbitrary size.

Simple manipulation of space-filling molecular models is hardly practicable considering the size of the problem, and a detailed computer-assisted modeling study would be required. This would also appear to be necessary if one wants to attempt to answer the intriguing question whether the observed homochirality of the HEL molecules within one particular TMA host sheet is due primarily to its apparently good complementarity with its mirror-image sheet, or whether this is more (or also) a property of the isolated sheet architecture itself. Quite naturally, this would first of all lead to the question of whether the non-planar puckering deformations of the TMA host sheets ('helix following') referred to above are energetically less costly if homochiral HEL guest molecules are to be accommodated, as compared to an achiral-sheet puckering mode supporting the uptake of HEL guest molecules of unlike chirality. Clearly, considerations of this nature are relevant if one envisages the feasability of creating $(TMA)_2 \cdot$ HEL monolayers with homochiral HEL guests (see below, *Sect. 3*).

It is well worth while to point out another interesting structural phenomenon of crystalline $(TMA)_2 \cdot HEL$, which may be referred to as 'helix alignment'. This means that the helical axes of all HEL molecules in $(TMA)_2 \cdot HEL$ are oriented in the same direction, *i.e.* they are all parallel (*Figs. 2* and *3*; for HEL, the helix axis may be chosen as running perpendicular to the mean plane of the molecule and thus coincident with the axis of maximum principal moment of inertia). In $(TMA)_2 \cdot HEL$, this helix alignment is crystallographically exact, *i.e.* the helix axes are parallel by crystal symmetry. If the helix axis is turned into a vector indicating the helical sense of the HEL molecule, then one may say that these helix vectors are anti-parallel for neighboring super-graphite sheets since the chirality of the HEL molecules alternates from one sheet to the next, as described above. It is to be stressed that in the crystals of HEL itself [6], the molecular helices are not aligned. Helix alignment may potentially give rise to interesting and extreme chiroptical and non-linear optical (NLO) properties, and the engineering of helix-aligned crystal architectures after the example of $(TMA)_2 \cdot HEL$ would thus promise to be a rewarding supramolecular challenge, as pointed out subsequently and in *Sect. 3*.

We have been thinking of further possibilities of engineering aligned molecular helices in helicene-containing crystals and concluded that this might straightforwardly be achieved in donor-acceptor π complexes. Crystals of such complexes are usually composed of stacks formed by alternating π donor and acceptor molecules, which are held together by face-to-face π contacts. Accordingly, racemic HEL was combined with the π acceptors 1,3,5-trinitrobenzene (TNB) and 3,5-dinitroenzoic acid (DNBA), respectively, in a 1:1 molar ratio in 1,2-dichloroethane as solvent. Good-quality, deep-yellow crystals could be obtained of the following 1:1 molecular complexes: HEL · TNB in monoclinic form, HEL · TNB in triclinic form, and HEL · DNBA. Even a molecular complex of HEL with the rather weak acceptor 5-nitroisophthalic acid (NIPA) could be crystallized (1:2 stoichiometry; deep yellow crystals from 1,2-dichloroethane/EtOH). Finally, black crystals of a 1:1 complex of HEL and 7,7,8,8-tetracyanoquinodimethane (TCNQ) were grown, again from 1,2-dichloroethane solution. The crystals of these 5 solid-state complexes were subjected to X-ray analysis (see *Exper. Part* and *Table*). Except for $(NIPA)_2 \cdot HEL$, the space groups of these crystals turned out to be centrosymmetric, showing that they are racemic and that no spontaneous enantiomer resolution had occurred in the crystallization processes. The

crystals of $(NIPA)_2 \cdot HEL$ take up the space group *Cc*, which is also achiral, of course. As we have seen above, this applies likewise to $(TMA)_2 \cdot HEL$ (space group *C*2/*c*, see *Exper. Part*). It should be noticed that despite the chiral space group ($P2_12_12_1$), HEL itself also (macroscopically) crystallizes practically without spontaneous resolution, which in this case is due to an unusual domain effect: The crystals are built up of domains in a special way, whose HEL molecules are homochiral, yet the chirality varies from domain to domain. This effect is not perceptible by conventional X-ray techniques, which cannot discriminate between enantiomorphic domains [9].

The four π donor-acceptor 1:1 complexes HEL·TNB(monoclinic), HEL·TNB(triclinic), HEL·DNBA, and HEL·TCNQ do indeed build up the expected donor-acceptor stacks in the crystal, as evidenced by the stereo views of *Figs. 6–8*. The 2:1 complex $(NIPA)_2 \cdot HEL$ is pretty different from these four 1:1 molecular compounds and more intricate (see below, *Fig. 9*). The crystals of HEL·TNB(monoclinic) and HEL·DNBA have one symmetry-independent HEL and nitroaromatic molecule each in the unit cell; those of HEL·TNB(triclinic) and HEL·TCNQ have two independent component molecules each in the cell, in both cases assigned to one and the same donor-acceptor stack. In all these four molecular complexes, we are thus faced with one type of stack, and all the stacks building up the crystals are related by symmetry. It may be seen from *Figs. 6–8* that the structure of the stacks is rather similar in the four cases. The face-to-face π complexed donor and acceptor molecules alternate, as does the chirality of the HEL π donors in the stacks. The donor-acceptor stacks are thus racemic in all these four 1:1 π complexes of HEL. The stacking axes are always parallel, and it readily emerges from *Fig. 6–8* that the HEL helices are aligned to a good degree of approximation. However, in contradistinction to $(TMA)_2 \cdot HEL$, this alignment is not enforced by crystal symmetry within the stacks. In the three 1:1 complexes involving nitroaromatic acceptors, the helices of HEL molecules in different stacks are strictly aligned *via* inversion centers and translational symmetry. This holds only partly in HEL·TCNQ since here symmetry-interconnection of stacks occurs also *via* glide planes.

The three 1:1 π complexes of HEL with nitroaromatic acceptors differ markedly in the mode the donor-acceptor stacks are disposed relative to each other in the crystal, and one may perhaps state that the three crystals are distinguished by their characteristic 'tertiary structures', so to speak. On the other hand, the tertiary structure of HEL·TCNQ, *i.e.*, its interstack contacts, is rather closely related to that of HEL·DNBA (see below). The differences in the inter-stack arrangements may perhaps best be worked out by considering the relative orientation and interaction of the HEL molecules in neighboring stacks. Basically, two types of HEL contact pairs may be discerned: One may be referred to as a centrosymmetric head-to-head HEL dimer with interdigitating molecular clefts and opposite chirality of the partners, the other as a head-to-tail HEL dimer with the middle part of one HEL molecule extending into the molecular cleft (groove) of the partner molecule and like chirality of both (*Figs. 6* and *7*). HEL contact pairs somewhat similar to the racemic head-to-head dimer may also be recognized in $(TMA)_2 \cdot HEL$ (*Figs. 2, b* and *c*). Now, inspection of *Figs. 6* and *7* shows that the monoclinic form of the HEL·TNB complex involves exclusively head-to-head HEL dimers across neighboring donor-acceptor stacks, the triclinic form of HEL·TNB both head-to-head and head-to-tail dimers (1:1 ratio), and the HEL·DNBA complex

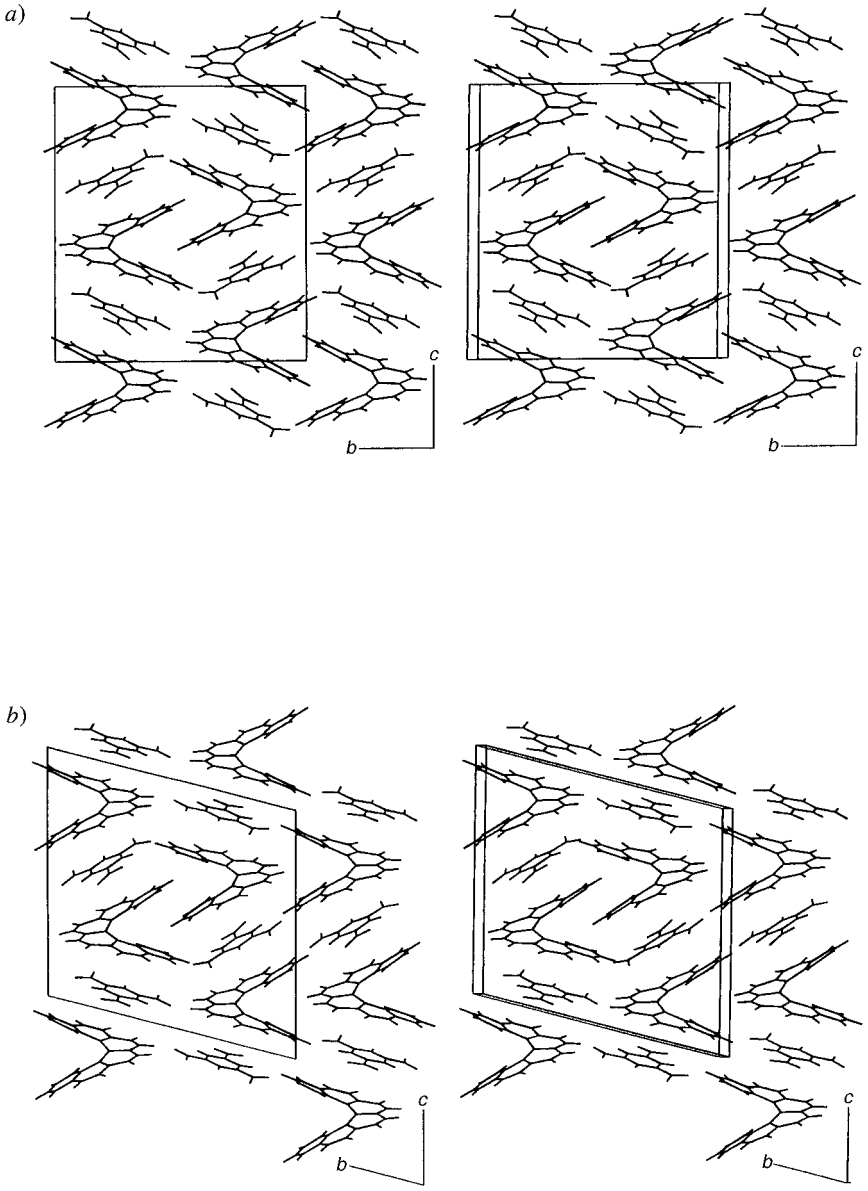

Fig. 6. *Stereoviews of the two crystal forms of HEL · TNB:* a) *monoclinic form and* b) *triclinic form*. The π donor-acceptor stacks run vertically. The chirality of the HEL molecules in the stacks alternates and the HEL-HEL contacts between neighboring stacks are exclusively head-to-head in the monoclinic form (see *a*), while both head-to-head and head-to-tail in the triclinic form (see *b*). The molecular helices of all HEL molecules are well aligned in both cases.

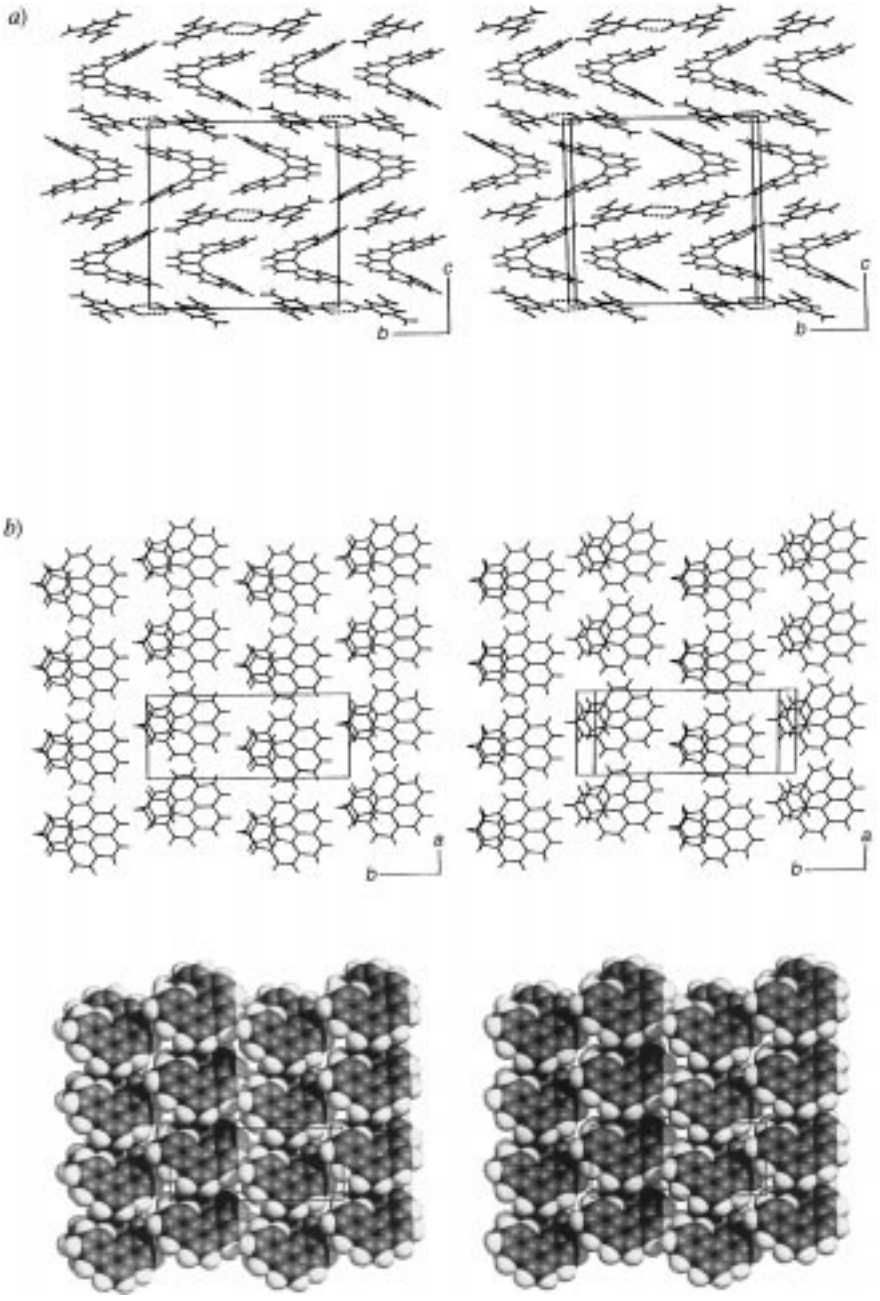

Fig. 7. *Molecular complex HEL · DNBA:* a) *Stereoview of the crystal structure* (*cf. Fig. 6*) *and* b) *stereoline and space-filling drawings of a layer of homochiral HEL molecules extending in the* a,b-*plane. Fig. 6:* the π donor-acceptor stacks are linked by pairwise H-bonds between the carboxy groups of DNBA (see *a*). All HEL molecules of the crystal architecture are helix-aligned; their chirality alternates in the stacks. The HEL · HEL contacts between neighboring stacks are exclusively head-to-tail.

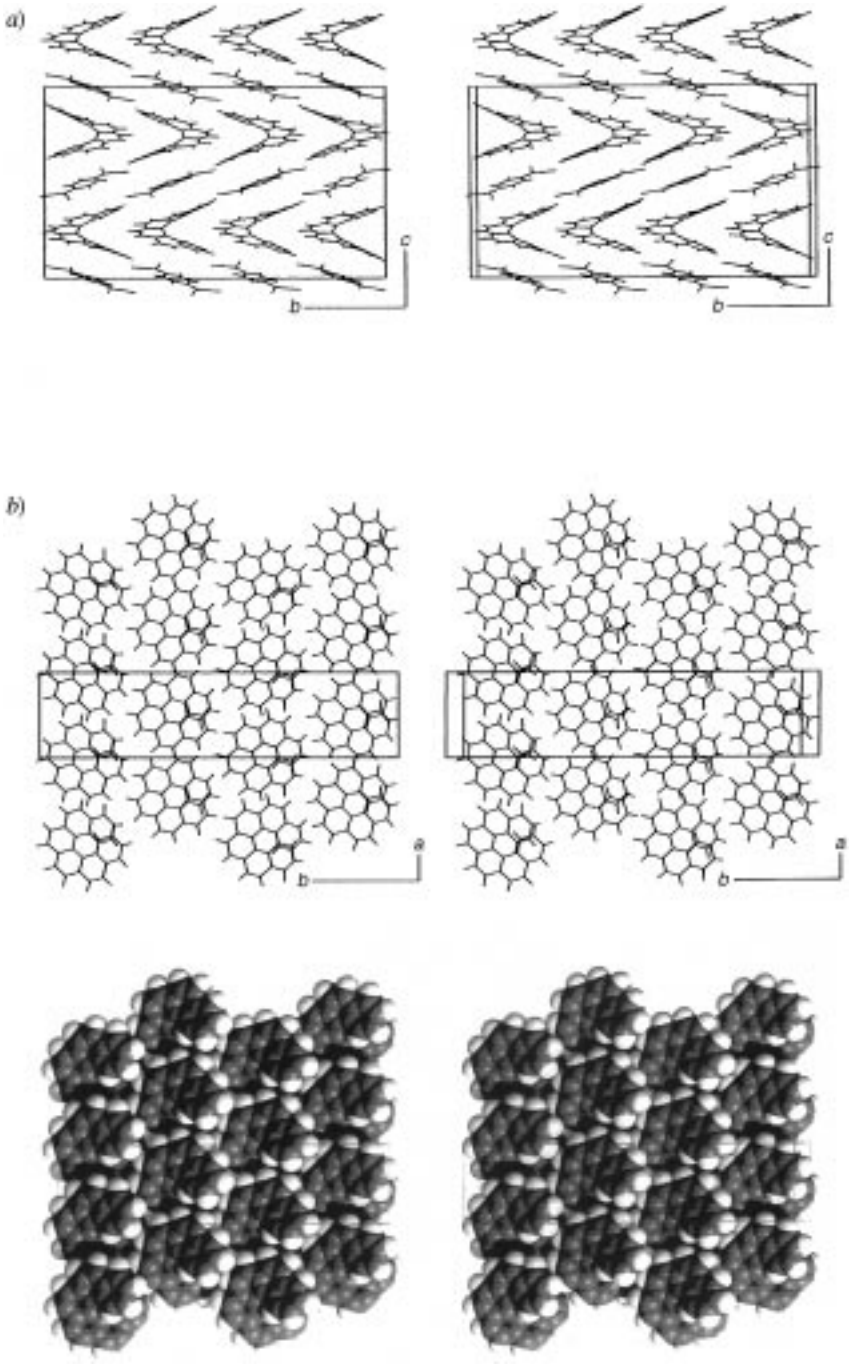

Fig. 8. *Molecular complex HEL · TCNQ*: a) *Stereoview of the crystal structure and* b) *stereoline and space-filling drawings of a layer of homochiral HEL molecules extending in the* a,b-*plane* (*cf. Fig. 7*). The π donor-acceptor stacks involve helix-aligned HEL molecules of alternating chirality (see *a*), and the HEL-HEL contacts are exclusively head-to-tail.

(as well as HEL·TCNQ) exclusively head-to-tail dimers. A consequence of the occurrence of both HEL dimers in the crystals of the triclinic form of HEL·TNB is the presence of each two symmetry-independent HEL and TNB molecules in the unit cell (see above and *Exper. Part*). It may also be seen that the two crystallographically different HEL·TNB complexes may be structurally transformed into one another by shifting suitable pairs (in the *b*,*c*-plane) of neighboring donor-acceptor stacks relative to each other along the stacking axis (crystallographic *c*-axis). The packing pattern of the HEL·DNBA complex may be developed similarly out of those of the two HEL·TNB complexes, with the triclinic form of the latter taking up a structure intermediate in character between the other two.

Of the three nitroaromatic donor-acceptor 1:1 complexes studied, the molecular compound between HEL and DNBA is particularly interesting, and accordingly its crystal structure merits some further comments. *Fig. 7* shows that the donor-acceptor stacks are linked by pairwise H-bonds between the carboxy groups of the acceptor acid molecules (O···O distance, 2.614(2) Å) to form sheets in the crystallographic *b*,*c*-plane. Of course, these sheets of H-bonded donor-acceptor stacks are racemic since the stacks themselves are heterochiral. The homochiral head-to-tail HEL dimers across neighboring stacks referred to above are in face-to-face π contact with one doubly H-bonded acceptor acid dimer. The acid dimers are roughly planar but some non-planar distortion is nevertheless perceptible (*Fig. 7*) leading to an improved adaptation to and π contact with the non-planar HEL molecules. *Vice versa*, the latter adapt appreciably to the preferentially planar acceptor dimers, *i.e.*, the HEL molecules are again flattened as compared to free HEL. The interplanar angle between the terminal benzene rings is only 47.3°, as compared to 58.5° in crystalline HEL itself. The flattening is not as extreme as in $(TMA)_2$·HEL (interplanar angle 42.0°; see above), but in this latter case, the HEL guest molecules are sandwiched by host acids from both sides. In the two TNB complexes, the HEL molecules are also flattened, but the effect is considerably smaller than in the two H-bonded complexes, as evidenced by interplanar angles of 53.6° (monoclinic form), and 53.8 and 57.5° (triclinic form; two independent HEL molecules). It thus appears that the intermediate flattening of HEL in the DNBA complex corresponds to the chemical intermediacy of this acid between TMA and TNB. Altogether, the H-bonding in the DNBA complex knitting together the donor-acceptor stacks in the sheets, corresponds to a brickwall pattern. Quite clearly, if H-bonding would exclusively occur within individual double-stacks, this would be a less favorable alternative since it would lead to HEL molecules sandwiched by H-bonded acceptor acid dimers from both sides and thus to poorer complementarity of the molecular partners. Finally, it therefore emerges that the H-bonding in $(TMA)_2$·HEL and HEL·DNBA supports the formation of extended planar aggregates of the acids, which exert a comparatively strong planarizing force upon the complexed HEL partners in order to improve interplanar stacking.

There is another and rather intriguing alternative to characterize the molecular packing in the crystals of the complex between HEL and DNBA. It becomes apparent by focussing the view on the distribution of the HEL enantiomers in the crystal rather than concentrating on the donor-acceptor stacks. It may be seen from the stereo views of *Fig. 7* that the HEL molecules of one particular chirality are organized in layers (in the crystallographic *a*,*b*-plane) roughly orthogonal to the sheets made up of the H-

bonded donor-acceptor stacks. The precise angle between the two layer types is equal to the crystallographic monoclinic β angle (101.4°; see *Table*). The crystal architecture of the HEL · DNBA complex may thus also be looked upon as being built up of homochiral HEL layers with interspersed doubly H-bonded acceptor acid dimers. The chirality of the HEL molecules of these layers alternates from layer to layer, and the HEL helices are well aligned with the helix axes approximately perpendicular to the layers. A line drawing and a spacefilling illustration of this beautiful supramolecular fabric is shown in *Fig. 7, b*. The homochiral, helix-aligned HEL layers in the DNBA complex may be compared with those present in the TMA complex as highlighted in *Fig. 3*. Two major differences are apparent: In the $(TMA)_2 \cdot HEL$ complex, the HEL molecules within a sheet are well separated by the embracing TMA host molecules, whereas in the HEL · DNBA complex, they are in comparatively close contact and completely fill the sheet by forming a pseudo-hexagonal array. Secondly, the layer separation is much smaller in the TMA complex than in the DNBA complex, the corresponding mean distances being 3.76 and 9.12 Å, respectively (*Figs. 2* and *7, a*). As well as in $(TMA)_2 \cdot HEL$, the helix alignment and the homochiral HEL sheets in the HEL · DNBA complex are significant as regards the engineering of interesting and extreme chiroptical and non-linear optical (NLO) properties in crystalline solids. In *Sect. 3* this is elaborated upon in some more detail.

It has already been noted above that the crystal architecture of HEL · TCNQ is largely similar to that of HEL · DNBA, and a comparison of *Figs. 7* and *8* illustrates this close supramolecular correspondence. The HEL molecules in the racemic donor-acceptor stacks of HEL · TCNQ alternatingly adopt left-handed and right-handed helicities and are again flattened relative to free HEL to improve the π contacts with the TCNQ partner molecules. For both independent HEL molecules, the interplanar angles between the terminal benzene rings amount to 47.2°, almost identical to the corresponding angle in HEL · DNBA (see above). As in HEL · DNBA, the HEL-HEL contacts in HEL · TCNQ are exclusively of the head-to-tail type with the middle part of one HEL molecule extending into the groove of the molecular partner of like helicity. This leads to essentially the same homochiral HEL sheets already encountered in HEL · DNBA (*Fig. 8, b*). The chirality of the HEL sheets in HEL · TCNQ again alternates from layer to layer with the helices of all HEL molecules well aligned. The layer separation of the HEL sheets in HEL · TCNQ measures 9.79 Å, 0.67 Å larger than in HEL · DNBA. Without going into quantitative detail, we note that this difference does not imply substantially shorter π donor-acceptor contacts in HEL · DNBA, but is chiefly due to the fact that in this latter complex, the HEL molecules protrude laterally out of the stacks appreciably as compared to HEL · TCNQ; a comparison of *Figs. 7, a* and *8, a*, will show this rather convincingly. It is finally pointed out that the homochiral HEL sheets in HEL · TCNQ and HEL · DNBA are not exactly alike but differ somewhat in the relative orientation of the HEL helices brought about by rotations around the helix axes. Furthermore, the packing of the HEL molecules in the sheets appears to be more compact in the TCNQ complex than in the DNBA adduct; compare *Figs. 7, b*, and *8, b*.

The arrangement of donor and acceptor molecules in segregated sheets in the crystals of HEL · TCNQ and the deep black color of the latter would appear to invite speculation as regards possible enhanced electric conductivity of this adduct. However,

spatial separation of π donors and acceptors is of course not the only important criterion to confer conductivity to organic materials, sufficient charge-transfer and π overlap being further essential prerequisites to this end. While the deep color of HEL · TCNQ might indicate appreciable donor-acceptor charge-transfer, inspection of *Fig. 8* shows virtually no π overlap among the TCNQ acceptor molecules and only poor contacts of this nature among the HEL donor systems. On the other hand, limited as they may be, the π contacts among the HEL molecules brought about by their special head-to-tail interdigitation *via* protrusion into each other's molecular clefts (*Fig. 8*), represent a rather unusual mode of supramolecular interaction, which cannot be readily assessed as regards its capacity of promoting conductivity. Thus, ultimately experiment will have to decide whether the electric properties of HEL · TCNQ might be of any interest. The prospects for enhanced electric conductivity of HEL · DNBA would seem still worse than for HEL · TCNQ taking into account the weaker acceptor strength of DNBA (much lighter yellow color of the former complex) and the less compact packing of the HEL molecules within their sheets in the DNBA adduct (*Fig. 7, b*), as noted in the previous paragraph.

We have described above molecular complexes of racemic HEL with TMA, TNB, and DNBA, and we see that in this series, one member is missing, *i.e.* an adduct between HEL and 5-nitroisophthalic acid (NIPA). We may then look upon a row of complexes of HEL with molecular partners derived from TMA through replacing none, one, two, or all carboxy functions by nitro groups, *i.e.*, formally the series *sym*-$C_6H_3(COOH)_{3-x}$-$(NO_2)_x$, with $x = 0, 1, 2, 3$. Of this series, NIPA ($x = 1$) is of course most closely related to TMA, and we thought that a complex between HEL and NIPA might be crystallizable by preserving some of the structural assets (C–H ··· O contacts, 'helix following'; see above) of $(TMA)_2$ · HEL, which would compensate for the relatively weak π acceptor properties of NIPA. As briefly noted earlier, we could indeed obtain deep-yellow X-ray-quality crystals of a complex of NIPA and (racemic) HEL. As for the TMA complex, its molar composition is 2 : 1 corresponding to the formula $(NIPA)_2$ · HEL, which might already indicate that we are on the right track with these suppositions; note that the HEL complexes with DNBA and TNB have 1 : 1 composition. The intriguing crystal structure of $(NIPA)_2$ · HEL turned out to be a fascinating architectural mélange between an inclusion complex à la $(TMA)_2$ · HEL and a π donor-acceptor complex à la HEL · TNB or HEL · DNBA, as expounded subsequently.

The complex $(NIPA)_2$ · HEL crystallizes in the non-centrosymmetric, yet achiral space group *Cc*, and is thus racemic. The large unit cell contains 24 NIPA and 12 HEL molecules, and we are thus faced with no less than 6 symmetry-independent NIPA and 3 independent HEL molecules, *i.e.*, with 168 independent non-H-atoms (see *Exper. Part*). The X-ray intensities were collected at low temperature (105 K, *Table*), and the structure could be solved without serious difficulties. Non-crystallographic, approximate extra translational and point symmetries in the unit cell became apparent. In particular, the molecules are approximately related through translations along the crystallographic *b* axis by one third of the respective cell edge. This is of some relevance in the context of crystal structural characterizations of $(NIPA)_2$ · HEL, as outlined subsequently. The X-ray structure refinement yielded one of the 3 independent HEL molecules with very high apparent temperature motion parameters, which could eventually only reasonably be treated as a rigid body with two split half-weight

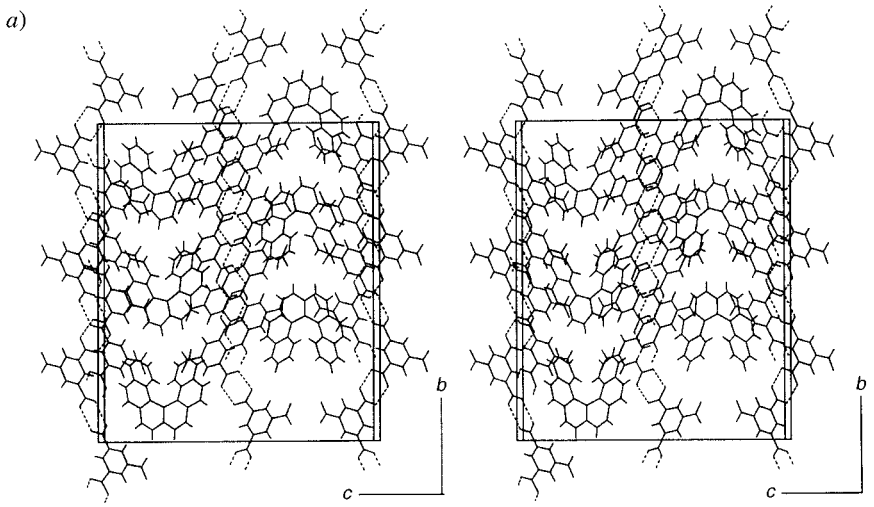

Fig. 9. a) *Stereoview of the crystal structure of (NIPA)$_2$·HEL with cell edges outlined.* Line and space-filling illustrations (mostly in stereo) of various relevant supramolecular aspects are given in *Fig. 9*. One of the 3 symmetry-independent HEL molecules is twofold orientationally disordered, of which a single averaged orientation is drawn instead (except in *Fig. 9, b*, see also main text). The O–H···O H-bonds in the line drawings are dashed. The nitro groups are not involved in O–H···O H-bonding and hence may easily be distinguished from the carboxy groups. In addition, the N-atoms are shown in white in the space-filling diagrams, as contrasted to the grey C-atoms.

orientations. In the illustrations provided by *Fig. 9*, this orientational disorder is indicated only in *Fig. 9, b*; in the other diagrams of *Fig. 9,* one single averaged orientation is drawn instead.

A convincing appreciation of the intricate crystal structure of (NIPA)$_2$·HEL is virtually impossible by a verbal description alone, and particular emphasis is thus to be laid upon an inspection of the stereo illustrations shown in *Fig. 9*. Gratifyingly, however, the supramolecular environment of the 3 independent HEL molecules and the 6 independent NIPA diacids is similar (*Fig. 9, b*), so we need not consider all these species individually; *cf.* the approximate extra symmetries of the unit cell pointed out above. If one were to attempt to develop a plausible structure of (NIPA)$_2$·HEL out of that of (TMA)$_2$·HEL, one might envisage as one out of many possibilities zig-zag chains of doubly H-bonded NIPA molecules created by cleaving a subset (*i.e.* a third) of parallel pairwise carboxy H-bond links in the TMA honeycomb sheets, preferentially those running vertically in *Fig. 3*, and replacing the carboxy groups affected by nitro functions. (Note that the O···O distance of a normal O–H···O H-bond is roughly equal to twice the *van der Waals* radius of the O-atom. Another intriguing possibility would be a crystal architecture involving HEL molecules surrounded by 6 NIPA molecules, which form a macrocyclic hexagonal ring held together by pairwise intercarboxylic H-bonds exactly as in the honeycomb cavities of (TMA)$_2$·HEL. A second set of twice as many HEL molecules would be required to join these large hexagons to make up for the observed 2:1 NIPA/HEL stoichiometry.) This modeling idea of creating NIPA zig-zag chains actually does conform to some extent to what is

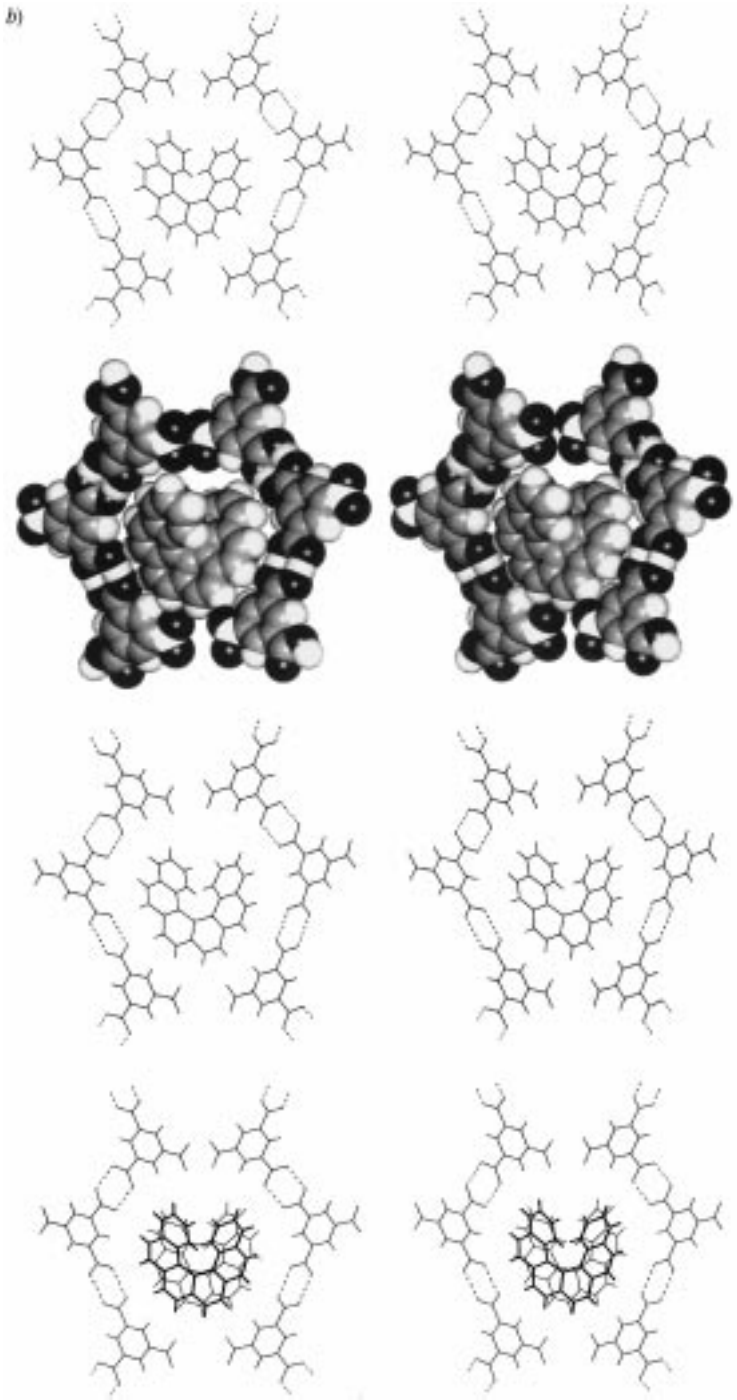

Fig. 9. b) *(NIPA)$_2$·HEL: View of HEL molecules surrounded by 6 NIPA molecules, showing the good 'helix-following' of the diacids* via *C–H···O contacts.* Line diagrams for all 3 independent HEL molecules and space-filling representation for the first of the two ordered species; bottom: illustration of the two orientations (heavy and light lines, resp.) of the disordered HEL molecule.

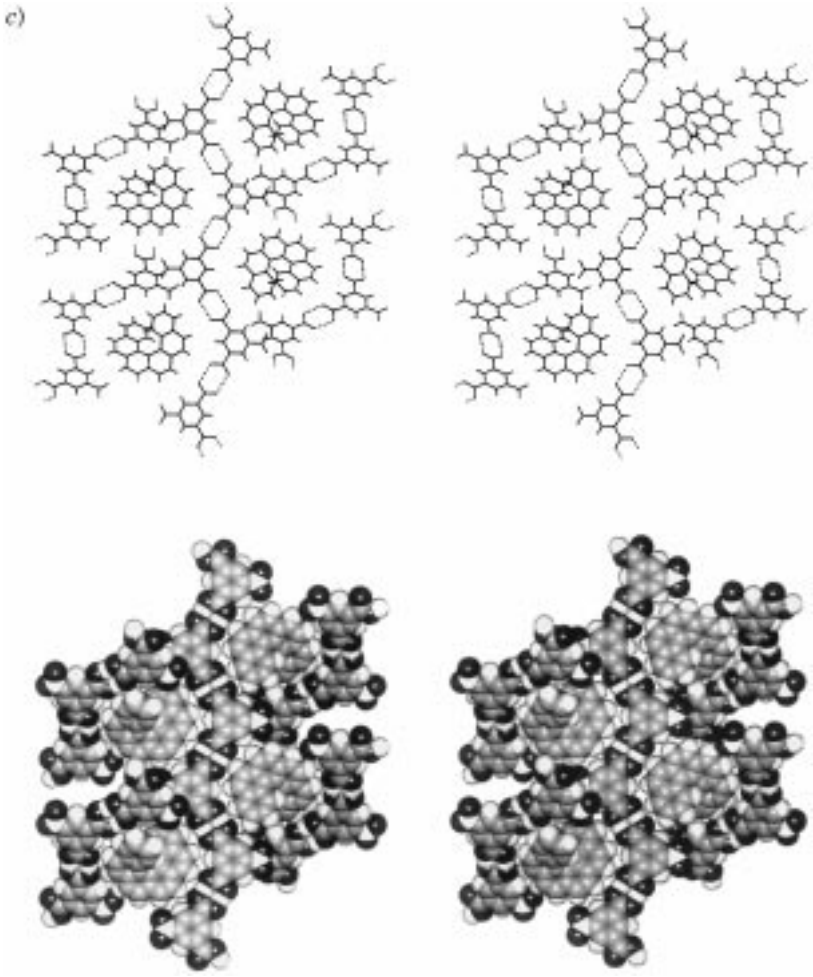

Fig. 9. c) *(NIPA)$_2$·HEL: 4 HEL molecules hooked to one common NIPA zig-zag chain and embraced by further diacid chains* (line and space-filling diagrams). Note the non-coplanarity of the crossed NIPA chains and the opposite chirality of the HEL molecules on both sides of the central NIPA chain.

observed, but represents only the first step of the structural rearrangements on passing from $(TMA)_2 \cdot HEL$ over to $(NIPA)_2 \cdot HEL$. The NIPA molecules in $(NIPA)_2 \cdot HEL$ are indeed doubly H-bonded *via* their carboxy groups to form zig-zag chains, but these chains are not coplanar as suggested by the above gedankenexperiment using $(TMA)_2 \cdot$ HEL as a lead structure. Neighboring NIPA zig-zag chains are in fact crossed in such a way as to embrace the HEL molecular partners at the crossing points *via* C–H···O contacts (*Fig. 9*). More specifically, we are faced with two sets of parallel zig-zag chains of H-bonded NIPA molecules running in the crystallographic *a*,*b*-plane, which cross each other. Within the sets, the NIPA molecules of the chains have face-to-face π contact. Through the crossing of the NIPA chains, an unfavorable juxtaposition of the

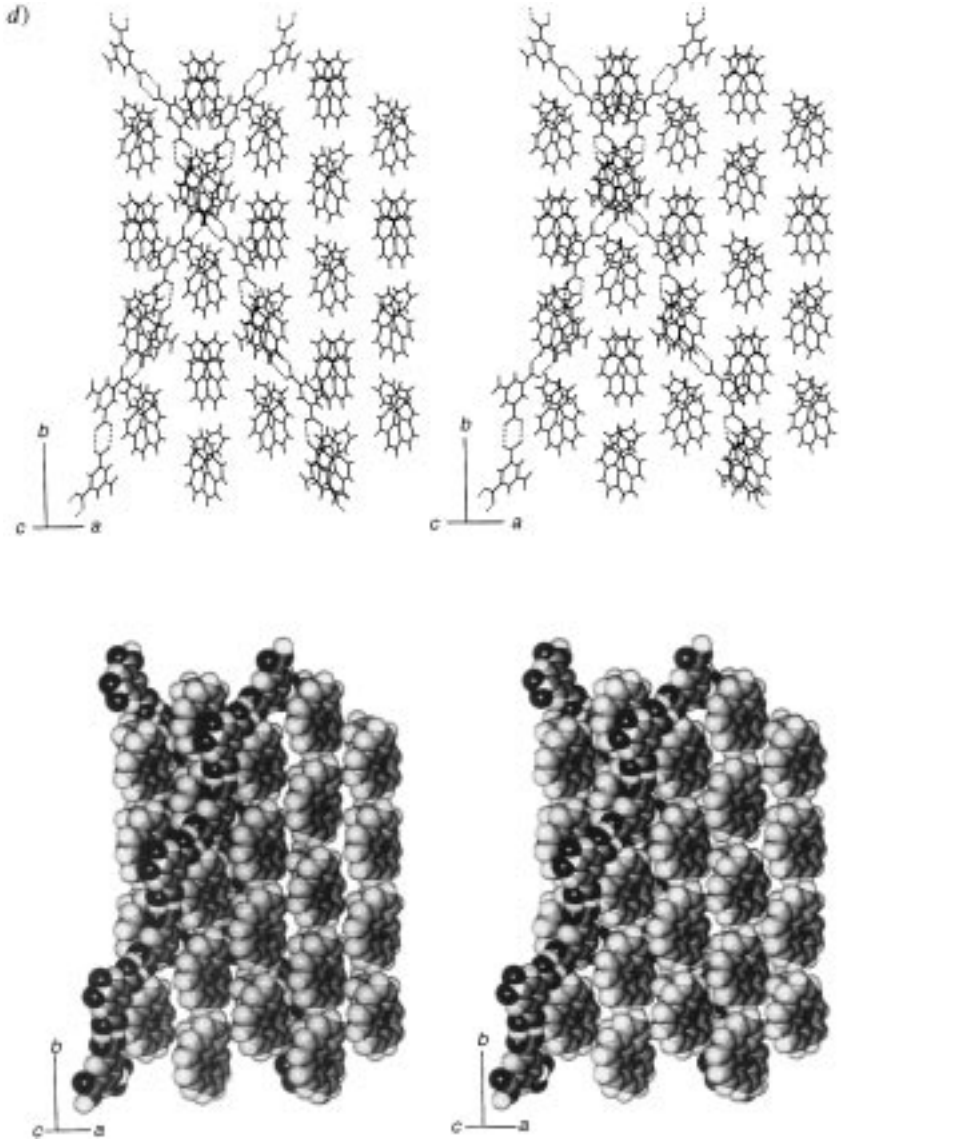

Fig. 9. d) *(NIPA)$_2$·HEL: Layer of homochiral, helix-aligned HEL molecules with two selected embracing NIPA zig-zag chains crossing each other* (line and space-filling drawings)

nitro groups is avoided and, most remarkably and elegantly, an almost perfect 'helix following' of the NIPA host chains with respect to the HEL guests is achieved. The NIPA chain crossing angle assumes just about the right magnitude to enable this virtually optimal mode of molecular recognition: Its actual value is given by the expression $2\tan^{-1}(a/b) = 47.5°$, which is close to the interplanar angle between the terminal benzene rings of the HEL molecules embraced by the crossed H-bonded

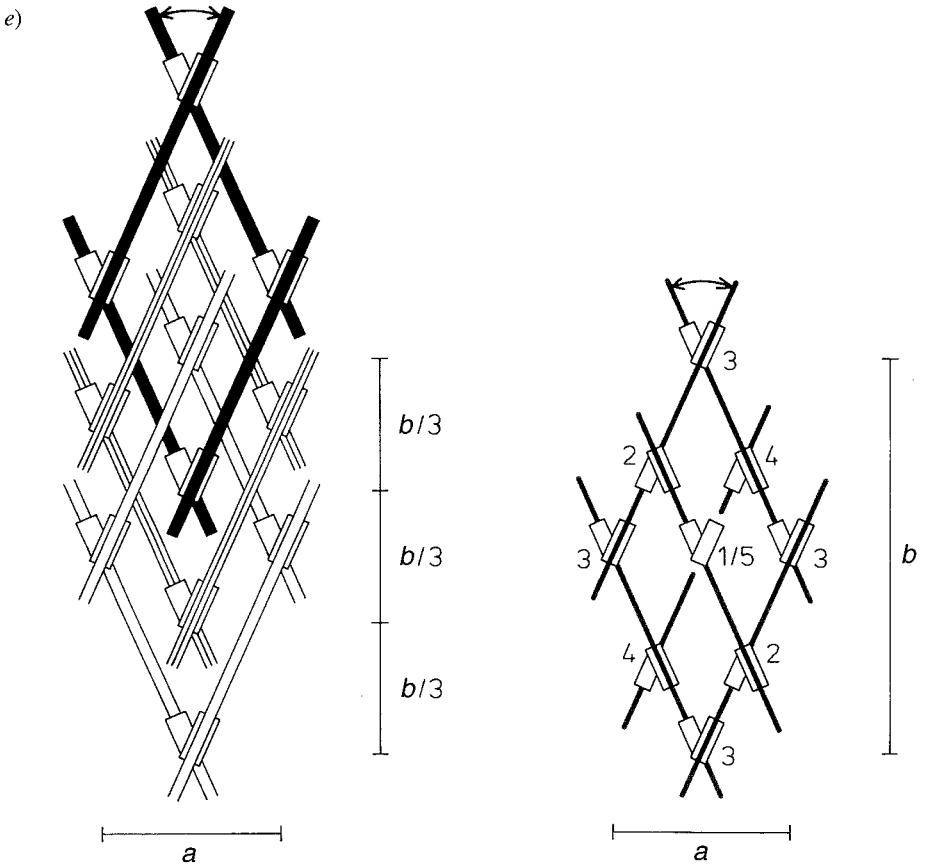

Fig. 9. e) *(NIPA)$_2$·HEL: Diagrammatic illustration of the crossed fence-type model* (left) *and the distorted-diamondoid interpretation* (right) *of the crystal structure.* The crossed, H-bonded NIPA zig-zag chains are represented as straight 'laths', the HEL molecules as interconnecting 'hinges' (*via* C–H···O contacts) at the crossing points. The metrical properties of the diagrammatic structural models are undistorted, and the crossing angle of the NIPA laths (47.5°) is indicated. Three interpenetrating crossed lath-and-hinge type fences are shown (left), and each is represented by 4 NIPA laths forming a rhomb (black, white, and shaded); note the homochirality of the HEL hinges arranged in a single layer. The diamondoid structural model (right) is represented by a single diagrammatic, distorted super-adamantane unit cut out of one of the 3 interpenetrating super-diamond networks. The HEL molecular hinges are assigned to 5 consecutive layers (indicated by numbers increasing with growing viewing distance), and the HEL chiralities alternate from layer to layer. Note that the 3-dimensional diamond networks may be constructed from the 2-dimensional crossed fences by appropriate stacking of the latter.

NIPA zig-zag chains. The observed interplanar angles of the two independent HEL molecules of (NIPA)$_2$·HEL refined without constraints are 46.9 and 48.2°, respectively, indicating a similar HEL flattening as observed in HEL·TCNQ and HEL·DNBA. The stereo views of *Figs. 9, b* and *c*, illustrate this beautiful example of host-guest complementarity rather impressively. The pattern of C–H···O contacts of the HEL molecules with the 6 surrounding NIPA molecules resembles that encountered in (TMA)$_2$·HEL (*Figs. 2* and *9*), although these contacts are less ideal in (NIPA)$_2$·HEL,

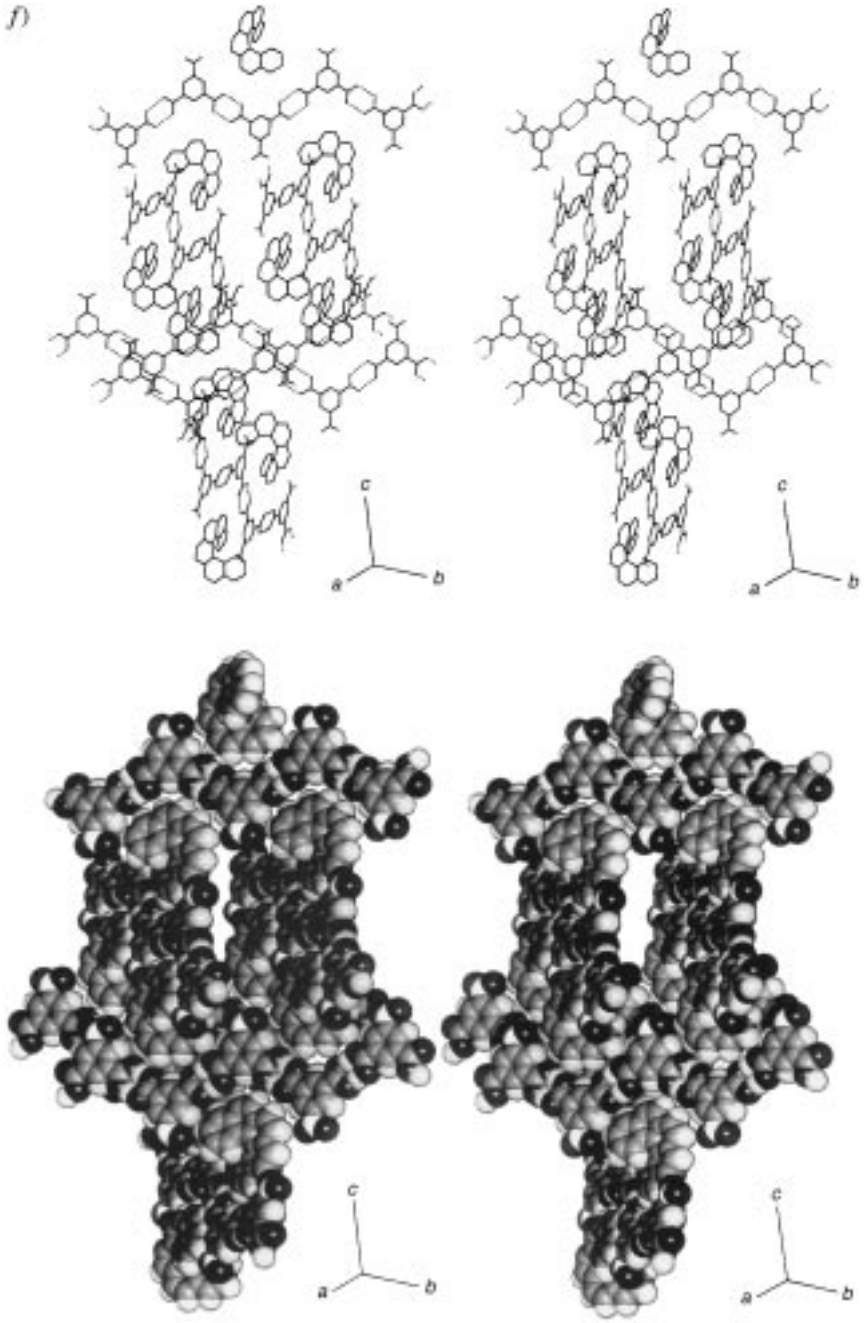

Fig. 9. f) g) *(NIPA)$_2$ · HEL: C–H ··· O and π donor-acceptor aspect, respectively, of the super-diamond networks* (line and space-filling diagrams); super-adamantane units are drawn for both cases, and the H atoms in the line drawings are omitted for clarity. Note the hollowness of the supramolecular architectures, which in the complete crystal structure is compensated by 3-fold interpenetration.

g)

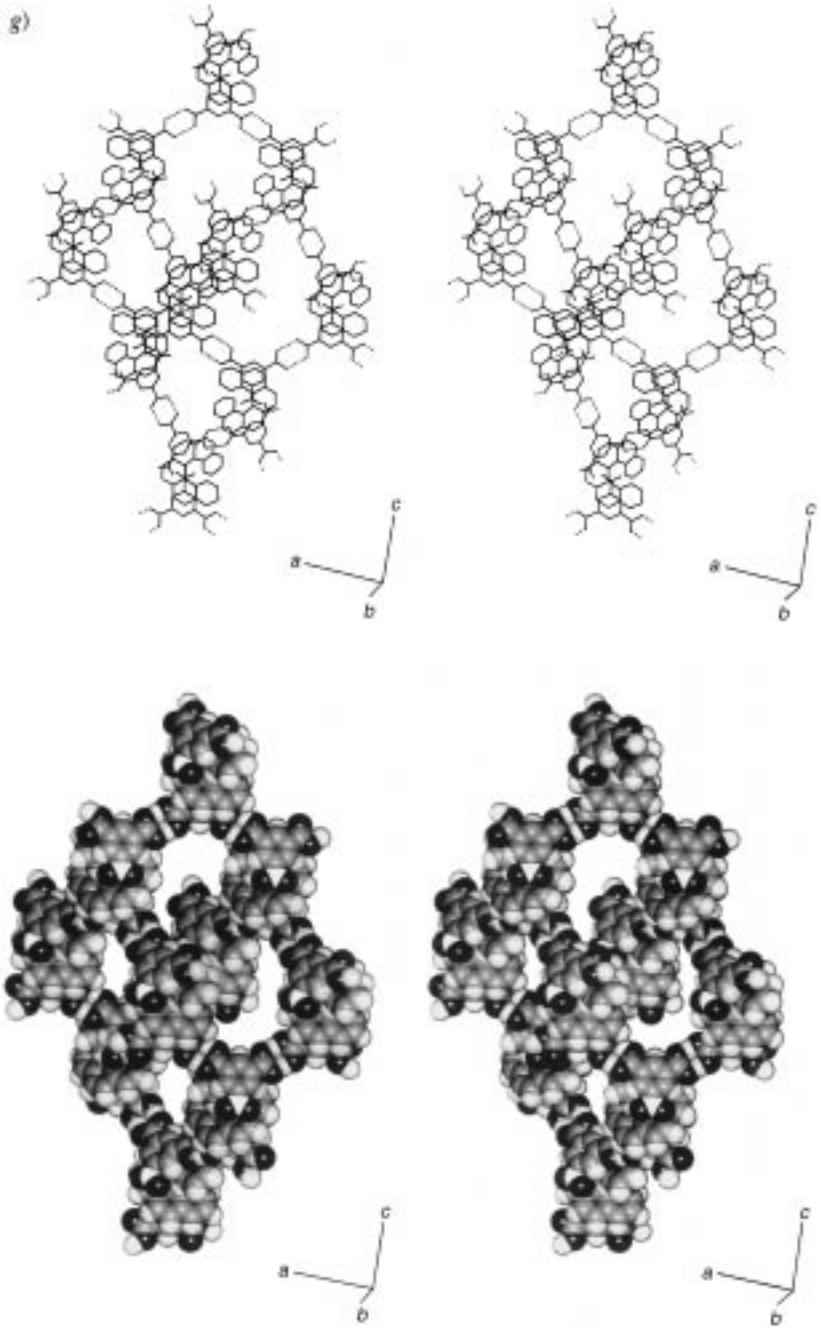

h)

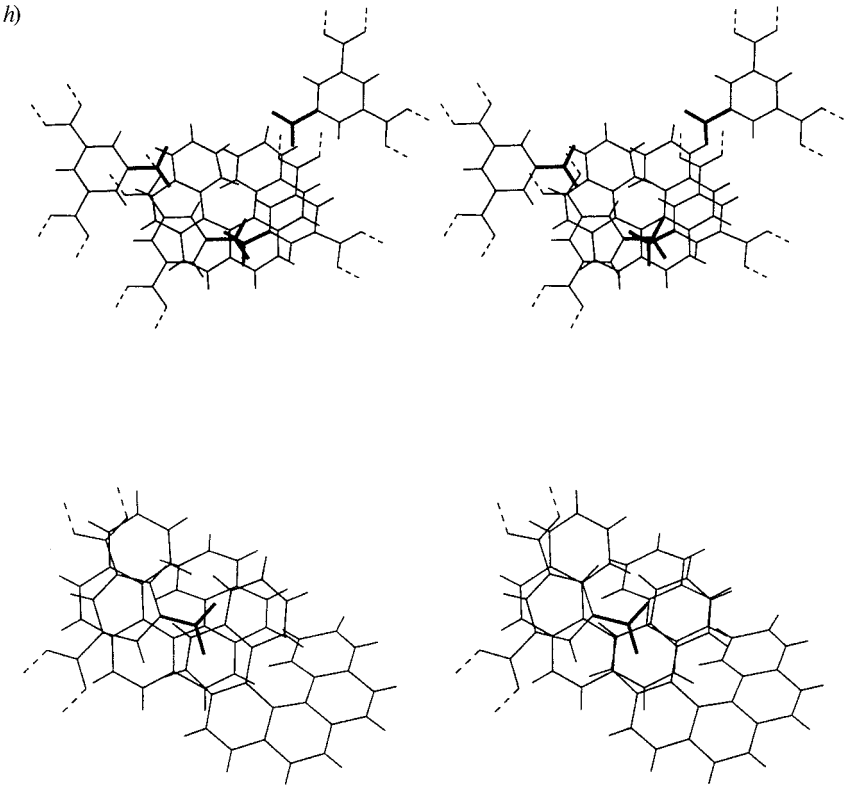

Fig. 9. h) *(NIPA)$_2$·HEL: π Donor-acceptor overlap of the HEL and NIPA molecules.* A HEL donor molecule surrounded by 4 NIPA acceptor molecules is shown (top) as well as a NIPA molecule with 2 HEL partners (bottom); nitro groups are drawn with thicker lines. Note that good π donor-acceptor contacts are chiefly established within more or less separate NIPA-HEL-NIPA units.

since the crossing of the NIPA zig-zag chains does not allow all C–H···O contacts to assume an essentially straight geometry. The honeycomb cages and their guests have crystallographic C_2 symmetry in (TMA)$_2$·HEL, yet only approximate C_2 symmetry in (NIPA)$_2$·HEL. This appears to be compensated by the even better 'helix following' of the NIPA host molecules than that of their TMA congeners. Specifically, *Fig. 9, b*, shows that the two ordered independent HEL molecules of (NIPA)$_2$·HEL establish rather straight C–H···O contacts analogous to *Fig. 1, a*, *via* one molecular branch, and bent C–H···O contacts analogous to *Fig. 1, b*, *via* the second branch. Furthermore, it may also be seen from *Fig. 9, b*, that this holds likewise for the two orientations of the disordered HEL molecule as resulting from their respective rigid-body refinements (see above).

The essence of the whole supramolecular architecture of (NIPA)$_2$·HEL may be likened to a fence consisting of crossed laths, representing the H-bonded NIPA chains, with the junctions between the laths provided by the HEL molecules, which may thus be viewed as molecular 'hinges' brought about by means of C–H···O contacts. However, a supramolecular fence of this kind is porous, and in actual fact 3 fences

interpenetrate to fill space effectively. These interpenetrating fences are related by approximate translations measuring *b*/3 as shown in *Fig. 9, e*. It may be readily seen that the HEL molecular hinges within such a triple fence form sheets and are necessarily helix-aligned and homochiral (*Fig. 9, d*). To build up the 3-dimensional crystal structure, the triply interwoven fences are stacked on top of each other by means of HEL hinges of opposite chirality, and we are finally faced with stacked, homochiral HEL sheets separated by the crossed NIPA laths, whereby the HEL molecules of neighboring sheets have opposite chirality (see below); *Fig. 9, e*, provides more insight. Accordingly, HEL molecules of neighboring sheets are related by crystallographic glide planes. Altogether, the lath-and-hinge fence-type view of the crystal structure of $(NIPA)_2 \cdot HEL$ leads to an intricate triply concatenated 3-dimensional network, which on closer inspection, however, reveals itself to be of an ingeniously organized, distorted diamondoid nature. The tetrahedral building blocks of these networks are represented by units consisting of one HEL molecule and two crossed NIPA molecules, with the latter oppositely $C-H\cdots O$ bonded to the branches of the central HEL partner. These moieties are doubly $O-H\cdots O$ bonded *via* the carboxy groups to build up the entire 3-dimensional diamond scaffold. As pointed out above for the crossed-fence model, which may be cut out of the diamond network and thus constitutes a substructure of it, the individual distorted diamond networks of $(NIPA)_2 \cdot HEL$ are highly porous and engage in a 3-fold interpenetration mode to fill space effectively. Again, *Figs. 9, e* and *f*, provide illuminating illustrations, in particular of a distorted super-adamantane unit cut out of a superdiamond network (*Fig. 9, f*), the hollow structure of which is clearly evident. The 3 concatenated diamond lattices are approximately translationally equivalent and may be transformed into one another through respective shifts along the crystallographic *b*-axis by an amount of about one third of the cell edge *b*.

The fact that the crystal structure of $(NIPA)_2 \cdot HEL$ may convincingly be characterized as a 3-fold distorted diamond architecture appears to us a veritably stunning result, and even with the knowledge of the detailed crystal structure of $(TMA)_2 \cdot HEL$ would have been virtually impossible to anticipate from first principles, similar to innumerable other hopeless cases of crystal structure prediction resulting in frequent failures of crystal-engineering attempts. The way the packing problem in $(NIPA)_2 \cdot HEL$ is dealt with by nature seems to us of even utter elegance, irrespective of the fact that many examples of interpenetrating diamond lattices in crystalline solids have been uncovered in the recent past. Referring to our own respective work, we note that the distorted 3-fold diamondoid crystal architecture of $(NIPA)_2 \cdot HEL$ may be compared to that of 3,3-bis(carboxymethyl)glutaric acid ('methanetetraacetic acid') [10a] or even better to that of the tetrahydrate of the tetrasodium salt of 1,3,5,7-adamantanetetracarboxylic acid [10b]. The latter structure consists of orthogonally crossed H-bonded H_2O chains cross-linked (again *via* H-bonds) by the tetracarboxylate tetraanions in such a way that a triply interpenetrating distorted diamond network of tetragonal symmetry with Na^+-occupied interstices emerges. Replacement of the H_2O chains in the anionic diamondoid scaffolds by H-bonded NIPA zig-zag chains and of the cross-linking tetracarboxylate tetraanions by HEL hinges, and finally lifting the tetragonal orthogonality constraint of the chain crossings, directly leads to the oblique monoclinic, triply interpenetrating diamondoid framework of $(NIPA)_2 \cdot HEL$.

We note finally that the diamondoid structural model of $(NIPA)_2 \cdot HEL$ as outlined above emphasizes its character as an inclusion compound, *i.e.*, its relationship with $(TMA)_2 \cdot HEL$ in regard of similar host-guest C–H···O contacts. Quite remarkably, it turns out that another set of triply interpenetrating, distorted diamondoid networks may be extracted from the supramolecular fabric of crystalline $(NIPA)_2 \cdot HEL$. This second, alternative diamondoid scaffold with like metrical and interpenetration properties again consists of crossed, H-bonded NIPA zig-zag chains which, however, are assigned to the HEL molecules in a different way such that the tetrahedral building blocks are now made up of HEL molecules sandwiched between two NIPA molecules via π donor-acceptor contacts (*Fig. 9, g*, see also further below). This second diamondoid interpretation of the crystal architecture of $(NIPA)_2 \cdot HEL$ thus emphasizes its character as a π donor-acceptor complex, *i.e.* its relationship with HEL · DNBA or HEL · TNB. The two characteristic aspects of $(NIPA)_2 \cdot HEL$, *i.e.*, inclusion compound *vs.* π complex, are thus seen to be paralleled structurally by an interesting diamondoid dichotomy. This means we are at the same time faced with a diamondoid 'C–H···O aspect' and a diamondoid 'π donor-acceptor aspect'. More insight may be gained by studying *Figs. 9, f* and *g*. It may be rather clearly seen that the close correspondence of the NIPA chain crossing angle and the HEL interplanar angle between the terminal 6-membered C-rings enables optimal π donor-acceptor contacts between HEL and NIPA in addition to and in combination with the optimal 'helix following' via C–H···O interactions (see above). Both these favorable supramolecular motifs are closely interrelated and interdependent, simply since the NIPA chains are stacked *via* face-to-face π contacts between the NIPA molecules, rendering parallel the planes of the NIPA chains within a stack (*Fig. 9, a*). That the supramolecular structural requirements of good 'helix following' and π donor-acceptor contacts in $(NIPA)_2 \cdot HEL$ may be simultaneously satisfied is of course ultimately also based on the more fundamental fact that the H atoms of HEL still more or less lie in the mean planes of the 6-membered C-rings to which they are attached. The non-planarity of the individual 6-rings is not excessive, irrespective of the pronounced non-planarity of the HEL molecule as a whole.

The present findings demonstrate that it may be quite rewarding to search for diamondoid structural patterns in crystalline solids. Even if, of course, not ubiquitously, they do appear to occur still more frequently than perhaps generally appreciated, and undoubtedly quite a few remain dormant in published crystal structures awaiting to be uncovered. Even to the crystal architecture of NIPA itself [11], which is also built up of crossed, doubly H-bonded zig-zag chains (crossing angle, 34.8°), some latent diamondoid character might perhaps be attributed.

Summarizing, we stress once again that, like in the other 5 molecular HEL complexes studied in the present work, the helices of all HEL molecules in $(NIPA)_2 \cdot$ HEL are once more well aligned, *i.e.*, the helix axes are all more or less parallel (*Fig. 9, d*). Moreover, the HEL molecules are again arranged in homochiral sheets (in the crystallographic *a*,*b*-plane; sheet separation, 12.61 Å) with alternating chirality from sheet to sheet. The supramolecular fabric of $(NIPA)_2 \cdot HEL$ was reduced above to the architecture of triply interpenetrating fences made up of crossed, hinged laths and stacked in diamondoid fashion, and this perspicuous pictorial model reproduces these alignment and chirality characteristics rather lucidly (*Fig. 9, e*). Within their sheets, the

HEL molecules are head-to-tail oriented and protrude into the clefts of neighbor molecules, similarly as in the HEL sheets of HEL·DNBA and HEL·TCNQ (*Figs. 9, d, 7,* and *8*). However, the helix axes of the HEL molecules in their sheets in $(NIPA)_2 \cdot HEL$ are not perpendicular to the plane of the sheets as in the HEL complexes with TMA, DNBA, and TCNQ, but rather run in the sheet planes (compare *Figs. 9, d*, and *3, 7,* and *8*). The packing of the HEL molecules in their sheets in $(NIPA)_2 \cdot HEL$ is relatively loose in such a way that niches open up between the hydrocarbon molecules, into which the nitro groups of the NIPA host molecules protrude. In this way, π donor-acceptor contacts are enabled, which expectedly appear less extensive, however, than in the HEL complexes with the stronger acceptors DNBA, TNB, and TCNQ. In the niches provided by the HEL sheets of $(NIPA)_2 \cdot HEL$, the nitro groups are in addition tied to the hydrocarbon molecules *via* seemingly rather favorable C–H $\cdots$ O contacts, as we are taught by *Fig. 9, d*. It is noted that the NIPA molecules in one particular H-bonded zig-zag chain are coplanar to a good degree of approximation. Small twisting deformations are nevertheless perceptible in the chains in order to allow a still better compromise among the steric requirements of the various host-guest contacts, *i.e.*, chiefly 'helix following' *via* weak C–H $\cdots$ O bonds and face-to-face π donor-acceptor interactions. That the requirements for optimal interactions of these two kinds may be simultaneously satisfied without *substantial* constraints, however, has been outlined above. As a whole, the crystal packing of $(NIPA)_2 \cdot HEL$ appears rather tight judging from the relatively high crystal density of 1.46 $g\,cm^{-3}$ (*Table*).

In conclusion, we notice that the complex $(NIPA)_2 \cdot HEL$ appears to 'borrow' good structural elements both from $(TMA)_2 \cdot HEL$ and the stronger donor-acceptor complexes already discussed: $(NIPA)_2 \cdot HEL$ shares its 2:1 stoichiometry with $(TMA)_2 \cdot HEL$ and has similar six-sided host chambers with excellent 'helix following' *via* C–H $\cdots$ O contacts and thus good host-guest complementarity; from the other π complexes the head-to-tail interdigitation in the HEL sheets is taken over and, of course, the face-to-face donor-acceptor π contacts. Compared to $(TMA)_2 \cdot HEL$, $(NIPA)_2 \cdot HEL$ is handicapped by less comprehensive O–H $\cdots$ O H-bonding, and compared to the other π complexes of HEL by the poorer π acceptor properties of NIPA. It may be argued that what matters in overcoming these disadvantages is the *combination* of the structural assets of both these types of molecular HEL complexes in $(NIPA)_2 \cdot HEL$ thus endowing it with sufficient stability. Accordingly, $(NIPA)_2 \cdot HEL$ might thus be referred to as a 'C–H $\cdots$ O assisted π donor-acceptor complex'. As to the weak π acceptor power of NIPA, it should finally not be overlooked that this deficiency is less serious than might appear on first sight since stoichiometrically we have two nitro groups per HEL in the 2:1 complex $(NIPA)_2 \cdot HEL$, *i.e.*, the same ratio as in the 1:1 complex HEL·DNBA. This might also account for the relatively deep color (dark yellow) of $(NIPA)_2 \cdot HEL$, which is qualitatively the same as that of HEL·DNBA. Inspection of *Fig. 9, h*, indeed shows that every HEL molecule in $(NIPA)_2 \cdot HEL$ has π contact with 4 surrounding NIPA molecules carrying each one nitro group; two of these contacts are substantial, while the other two, *i.e.* those *via* the nitro groups in the region of the HEL cleft, are rather limited. *Vice versa*, every NIPA molecule has π contacts with two neighboring HEL molecules, one substantial and the other poor. In HEL·DNBA, the HEL molecules in the donor-acceptor stacks have good π contact with two DNBA acids (*Fig. 7*) carrying each two nitro groups, and the latter are sandwiched

between two HEL molecules *via* good π contacts. In other words, in $(NIPA)_2 \cdot HEL$, the donor-acceptor π contacts are largely localized within isolated NIPA-HEL-NIPA sandwiches, whereas in $HEL \cdot DNBA$, we have endless donor-acceptor stacks with every DNBA molecule engaged in two sandwiches of the type $(DNBA)_{1/2}$-HEL-$(DNBA)_{1/2}$. Thus in the first case, the NIPA molecules essentially have one-sided π contacts with HEL, whereas in the latter case the DNBA molecules have good π contacts *via* both sides of the molecular plane.

We thought it possible to create a 1:1 molecular complex of phenanthrene (PHEN) and NIPA bearing in mind that the PHEN skeleton is a substructure of both HEL and COR. Indeed the systematic name of HEL, phenanthro[3,4-*c*]phenanthrene, conveyes that the molecule is composed of two fused PHEN halves. PHEN provides half the CH periphery of HEL and COR and should fit perfectly well into the indentations offered by the doubly H-bonded zig-zag chains of NIPA *via* 6 good C–H···O contacts. These indentations of the NIPA chains clearly represent essentially one half of the hexagonal cavities of the TMA honeycomb sheets as occurring in $(TMA)_2 \cdot HEL$ and $(TMA)_2 \cdot$ COR. The complex $PHEN \cdot NIPA$ could indeed be readily crystallized in the shape of pale-yellow needles (see *Exper. Part*) and proved to build up the expected crystal structure (*Fig. 10*). $PHEN \cdot NIPA$ takes up space group *P*-1 with each two crystallographically independent PHEN and NIPA molecules (*Table*), which are similar as regards their C–H···O contacts, yet experience different π contacts (*Fig. 10, b*). The independent molecules belong to one and the same PHEN-loaded NIPA zig-zag chain such that all these chains in the crystal are equivalent. The PHEN-carrying NIPA chains are arranged in largely, yet not entirely, planar sheets stacked in such a way as to allow good donor-acceptor π contacts (*Fig. 10, b*), which give rise to the light-yellow color of the crystals. The PHEN molecules are rotated somewhat out of the symmetric orientation providing optimal C–H···O contacts, for reasons difficult to assess (average C···O distance of these contacts, 3.651 Å; *Fig. 10, a*). The planes of the PHEN molecules in $PHEN \cdot NIPA$ are thus seen to be all parallel to a good degree of approximation, *i.e.* they are well aligned, in contradistinction to PHEN itself [12], in the crystals of which the molecular planes are severely inclined. The structural interrelations between $PHEN \cdot NIPA$ and $(NIPA)_2 \cdot HEL$ as well as $(TMA)_2 \cdot HEL$ are evident as a comparison of *Figs. 10*, *9, c*, and *3* convincingly illustrates. Further comparison with *Fig. 1, a*, demonstrates the structural connexions of $PHEN \cdot NIPA$ and $(TMA)_2 \cdot COR$, which brings us back to the outset of the present study. Thus the structure of $PHEN \cdot$ NIPA once again supports our earlier conclusion that the preferred orientation of COR in the TMA complex should very likely correspond to that of *Fig. 1, a*, which excels in the better C–H···O contacts as compared to the arrangement of *Fig. 1, b*. Finally, the structural similarities of $PHEN \cdot NIPA$ and the complex $(TMA)_2 \cdot pyrene \cdot (EtOH)_2$ [1c] cited earlier should be pointed out considering that the C-skeleton of PHEN is a substructure of pyrene, which in turn is a building block of COR.

It is not entirely without surprise that the complex $PHEN \cdot NIPA$ can indeed be easily crystallized considering the weak π-donating and π-accepting capabilities of PHEN and NIPA, respectively. As for $(NIPA)_2 \cdot HEL$, the deeper reason for $PHEN \cdot$ NIPA to acquire sufficient stability probably is again related to the fact that both molecular partners are held together not only by (weak) donor-acceptor π contacts but also through a very favorable pattern of C–H···O contacts. It seems justified,

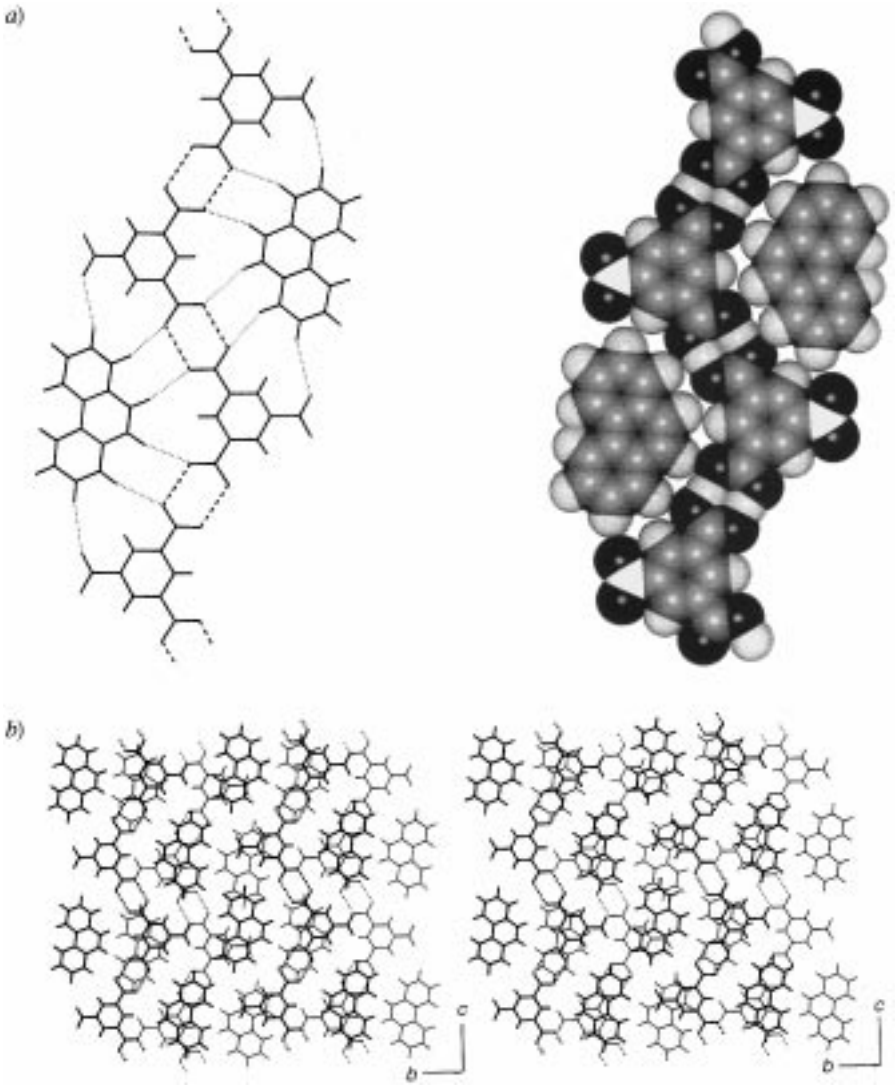

Fig. 10. a) *X-Ray crystal structure of PHEN · NIPA: part of a doubly H-bonded zig-zag chain of NIPA molecules carrying PHEN partner molecules* (line and space-filling views). The discrimination of nitro and carboxy groups is rather obvious; see legend of *Fig. 9*. O–H···O H-bonds dashed, C–H···O contacts dotted in the line diagram; compare with *Figs. 1, a, 2, a,* and *9, a* and *c*. b) *Stereorepresentation of two adjacent PHEN · NIPA layers composed of NIPA zig-zag chains loaded with PHEN molecules.* Illustration of π donor-acceptor overlap.

therefore, also to refer to PHEN · NIPA as a 'C–H···O assisted π donor-acceptor complex'. It is worth noting that co-crystallization of NIPA and anthracene (ANTH), which is a stronger π donor than PHEN, produced a crystalline ANTH-NIPA complex, if at all, only in low yield. In several crystallization runs, either no complex formation was observed or small amounts of small yellow crystals appeared together with a large excess of unchanged colorless component crystals. These yellow crystals may possibly

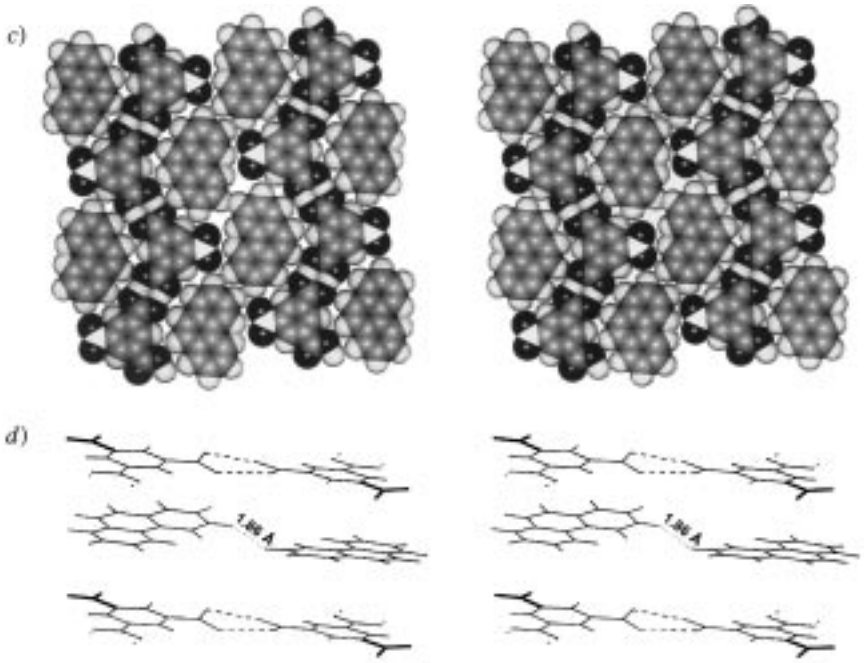

Fig. 10. c) *Space-filling stereoview of a PHEN · NIPA layer.* Note the short H ··· H contact in the center of the drawing (overlapping H spheres). d) *Stereoillustration of the close approach of two PHEN molecules within a layer, with short H ··· H contact indicated.* The PHEN molecules are sandwiched between NIPA molecules of two H-bonded zig-zag chains of neighboring layers. Nitro groups are drawn with thicker lines.

correspond to an ANTH-NIPA complex, but no X-ray structure could so far be obtained due to insufficient size and quality of the crystals. The co-crystallizations of PHEN and NIPA produced crystals of the PHEN · NIPA complex quantitatively. Clearly, the structural complementarity of the NIPA zig-zag chains as regards good C–H ··· O contacts is markedly poorer with ANTH than with PHEN since the linearly annellated ANTH molecule is not superimposable on to the outer rim of HEL or COR. The stability of the (putative) ANTH-NIPA complex thus may in the solid state well be lesser than that of PHEN · NIPA since it does not benefit from a sufficient C–H ··· O assistance, which is not compensated by the better π donor capabilities of ANTH. Moreover, the crystal packing of PHEN itself appears to be less favorable than that of ANTH, as indicated by the much lower melting point of PHEN (101° *vs.* 218° for ANTH), and this should lead to further stabilization of PHEN · NIPA relative to the (putative) ANTH complex. The apparent preferred formation of PHEN · NIPA relative to an ANTH complex of NIPA could in principle be utilized for separating PHEN and ANTH. As is well known, this separation is not possible by fractional distillation since both hydrocarbons have very similar boiling points. Likewise, PHEN · NIPA could be of use for purification of raw technical PHEN, which contains ANTH as the major impurity.

There is one more feature of the crystal structure of PHEN · NIPA, which is worth to be commented on. Inspection of *Fig. 10, c*, which provides a space-filling view of a

PHEN · NIPA layer, shows that two H-atoms of neighboring PHEN molecules (in the center of the diagram) are virtually 'bumping into each other', suggesting a very short intermolecular H···H contact. From the refined positions of the two H-atoms involved, indeed the rather short H···H distance of 2.11(4) Å is obtained (associated C···C distance, 3.849(5) Å). However, since, as usual, the two C–H bonds concerned result markedly shortened from the X-ray refinement (C–H bond lengths only 0.89(3) and 0.97(3) Å, resp.), the true H···H distance is expected to be substantially shorter than the X-ray value. Normalizing the C–H bonds to a length of 1.08 Å gives a corrected H···H distance of only 1.84 Å, which is extremely short indeed. Of course, the H-positions from the X-ray measurement are not very reliable, and a closer analysis in fact shows that one of the two congested H-atoms is bent out of the plane defined by the bonded C atom and the two C atoms attached to the latter, in such a way as to shorten the H···H contact still further. This is rather unreasonable, and the corrected X-ray H···H distance appears somewhat too short. A better estimate is probably obtained from H-positions calculated from the reliable X-ray C-positions involved, using standard stereochemical criteria (C–H length 1.08 Å, bisecting C–H bond in the plane of the bonded C-atoms). The H···H distance thus derived amounts to 1.86 Å. This value might still be somewhat too small since the H atoms could indeed experience some out-of-plane bending (pyramidalization) deformations, but opposite to those resulting from the X-ray refinement! Certain bond-angle deformations at the C atoms bonded to the close H atoms as well as small compressions of the C–H lengths are also conceivable to alleviate the intermolecular non-bonded H···H repulsion. The respective effects are not expected, however, to lead to an increase of the calculated H···H distance by more than a few hundredths of an Å. Strictly speaking, the calculated short H···H distance should thus nevertheless be referred to as an estimated lower limit, and neutron diffraction would have to be invoked for still more reliable conclusions. Its value is more than 0.5 Å shorter than the *van-der-Waals* diameter of H and comes rather close to the shortest reliably measured intramolecular H···H distances as occurring in sterically congested hydrocarbons [13].

Inspection of *Fig. 10* quite convincingly suggests that the present short intermolecular H···H contact between two neighboring PHEN molecules within one and the same PHEN · NIPA layer is responsible for their rotation away from the orientation allowing optimal C–H···O contacts (see above). At the same time, it may also well be that the observed deviations from coplanarity of the molecules in a PHEN · NIPA layer are likewise due to the H···H repulsions between neighboring PHEN molecules leading to some reduction of the associated strain (see below). It should be noted that the NIPA zig-zag chains are not entirely coplanar either and some twisting of the doubly H-bonded carboxy groups is observed (*Fig. 10, d*). Finally, the C-skeletons of the PHEN molecules themselves deviate significantly from planarity, again in such a way as to increase the short H···H contact (maximum separation of PHEN C-atoms from best molecular plane, 0.066(4) Å). By careful examination, this is qualitatively perceptible even from *Fig. 10, d*. Obviously, the question arises as to why in the crystal structure of PHEN · NIPA such an extremely short intermolecular H···H contact is tolerated. Again from an inspection of *Fig. 10, b* and *c*, it may be inferred that a larger separation of the PHEN molecules in the layers would lead to open spaces between them and the NIPA nitro groups and thus poorer respective C–H···O contacts.

Secondly, the PHEN molecules are sandwiched between H-bonded NIPA zig-zag chains *via* π donor-acceptor interactions, and the preferred (but, as noted, not completely established) planarity of the NIPA chains forces the PHEN molecules likewise to observe, within certain limits, coplanarity (*Fig. 10, d*). Clearly, if the PHEN molecules could escape from coplanarity in *substantial* measure, this would be beneficial for alleviating the intermolecular non-bonding H···H repulsions. These considerations, finally, also show rather nicely how the interplay, *i.e.* cooperativity, of H-bonding, C–H···O contacts, and π donor-acceptor interactions in PHEN·NIPA altogether essentially leads to a crystal architecture composed of sheets approaching, albeit not reaching, planarity, which is robust enough to sustain very appreciable intermolecular H···H repulsions in the layers.

Crystals of (D_{10})PHEN·NIPA were grown and subjected to an X-ray measurement ($R_1 = 0.056$ for 3917 significant reflections) to see whether the deuteration leads to a detectable further reduction of the short H···H contact (or rather D···D contact) between the PHEN molecules, due to the smaller effective size of D as compared to H. Based on the refined C-positions of the (D_{10})PHEN molecules, the short D···D contact is indeed calculated smaller than the corresponding H···H contact, but only by 0.008 Å (associated C···C distance 0.013(7) Å smaller than in the non-deuterated complex; the short D···D and C···C distances in the deuterated complex are thus 1.85 and 3.836(7) Å, resp.). This is on the verge of statistical significance, and we do not discuss any further details of our standard X-ray measurement on (D_{10})PHEN·NIPA. More experimental effort would have to be invested to definitely establish whether or not deuteration of PHEN leads to a measurably shortened D···D contact in the crystalline complex with NIPA. We note further that a routine IR spectrum of crystalline PHEN·NIPA (CsI pill) did not reveal a band indicating an enhanced C–H stretching frequency, which may be expected as a consequence of the short intermolecular H···H contact between the PHEN molecules.

In addition to $(TMA)_2$·COR, the primer of this work (see *Sect. 1*), we have, for the purpose of further comparisons, also crystallized molecular complexes of COR with TNB, DNBA, and NIPA, applying suitable diffusion procedures (see *Exper. Part*). We confine our respective discussion basically to some qualitative annotations, however, and do not give here much quantitative details. The compositions of these 3 new COR complexes correspond to the formulations COR·TNB, COR·DNBA, and $(NIPA)_2$·COR, and we notice that the altogether 4 COR complexes considered have the same stoichiometries as the corresponding HEL adducts. The crystals of COR·TNB and COR·DNBA are needle-shaped with deep brown-red and orange-yellow colors, respectively. $(NIPA)_2$·COR forms rosette-like groups of orange-red crystals with curved edges. As with the TMA complexes of COR and HEL, the crystal colors of the π donor-acceptor complexes of COR are thus again deeper than those of the analogous HEL adducts, and the $(NIPA)_2$·COR complex anew strikes the eye by its relatively deep color as compared to the adducts with the stronger π acceptors, possibly again due to its 2:1 stoichiometry. The crystal structures of COR·TNB and COR·DNBA could be solved X-ray analytically (both monoclinic, space group $P2_1/c$, 4 + 4 molecules in the unit cell), that of $(NIPA)_2$·COR resisted respective attempts. The analytical failure in the latter case is not entirely clear; X-ray photographs show rather good crystallinity, although the reflections partly do exhibit irregular shapes and are sometimes equipped

with 'tails' indicating disorder phenomena. The stoichiometry of $(NIPA)_2 \cdot COR$ was established by NMR spectroscopy. The crystals of $COR \cdot TNB$ and $COR \cdot DNBA$ also do not possess entirely ordered structures inasmuch the COR molecules suffer from orientational disorder, with two preferred orientations related by rotations around the six-fold molecular axes. Thus, we see that replacement of COR by HEL in the complexes with all the molecular partners of the compared series, *i.e.*, TMA, TNB, DNBA, and NIPA, leads to increased structural order, to the point that the crystal structures of $(TMA)_2 \cdot COR$ and $(NIPA)_2 \cdot COR$ could not even be solved.

In the crystals of $COR \cdot TNB$ and $COR \cdot DNBA$, the usual parallel donor-acceptor π stacks are encountered, with the molecular planes not exactly at right angles to the stacking axes; the deviations amount to roughly 20 and 10°, respectively. In COR itself, the molecules also form π stacks, but the inclination of the molecular planes with respect to the stacking axis is larger, around 40° [3]. Because of these inclinations and the space group symmetries, the molecular disks of the COR molecules are not aligned, *i.e.* their normals are not all parallel, in contradistinction to the (very probably) aligned COR disks in $(TMA)_2 \cdot COR$ and the molecular helix alignment in the HEL adducts. In the COR π donor-acceptor complexes, as well as in COR itself, the COR disks of one half of the π stacks are aligned in one direction, and those of the other half in a different second direction. It is striking, however, that in $COR \cdot DNBA$, disk alignment is best approximated since the COR molecular planes are fairly closely orthogonal to the stacking axes, as noted above. This probably has to do with the fact that the DNBA molecules of the complex occur in pairs doubly $O-H \cdots O$ H-bonded *via* their carboxy groups. The extended H-bonded DNBA dimers strive for coplanarity, of course, and this should quite generally also encourage a more coplanar disposition of their COR partner molecules, *i.e.*, increased disk alignment. The flattening of the HEL molecules found in $HEL \cdot DNBA$ apparently is of related origin (see above). However, the approximate disk alignment in $COR \cdot DNBA$ does not mean that the COR molecules are arranged in sheets. This is in contrast to $HEL \cdot DNBA$, which involves helix-aligned HEL layers, as we have seen. It is noted, finally, that the arrangement of the parallel donor-acceptor stacks in the crystals of the compared COR and HEL adducts is similar, following a pseudo-hexagonal pattern.

3. Conclusions. – In TMA itself, the large hexagonal cavities of the H-bonded honeycomb layers are filled through multiple self-interpenetration of the sheets [1a]. The present work shows that this interpenetration does not generally prevent the uptake of molecular guests by TMA, but may be broken if molecular partners are offered, whose shape is sufficiently complementary to the hexagonal TMA chambers, and which can well bind non-covalently to the carboxy O-atoms lining up the cavities. In the case of the molecular complex $(TMA)_2 \cdot COR$, the host-guest fit appears to be almost perfect, and virtually no structural adaptation of the molecular partners is necessary for optimal molecular recognition. The supramolecular binding of the COR guest molecules by the TMA host thus corresponds to a more or less ideal lock-and-key scenario. On the other hand, the binding of HEL by TMA is accompanied by substantial cooperative structural adaptations of both molecular partners, which are not well represented by the rigid lock-and-key model [14], but rather follow a mechanism of mutually induced fit [8]. The extent of the structural distortions of both

TMA and HEL, *i.e.*, the puckering of the TMA super-graphite sheets and the HEL flattening, is surprisingly large, and it appears well possible that the respective flexibility of host and guest is the decisive factor to confer stability upon the molecular complex $(TMA)_2 \cdot HEL$.

The present study provides a number of lucid examples of how molecules may be aligned in the solid state through suitable supramolecular engineering. In $(TMA)_2 \cdot COR$, the hydrocarbon molecules are (very probably) all coplanar, *i.e.* disk-aligned, whereas in crystalline COR itself, the molecules follow a herring-bone pattern with oblique molecular planes. More significantly as regards interesting material properties, in the complex $(TMA)_2 \cdot HEL$, the HEL molecules have their helix axes perfectly aligned and are arranged in homochiral sheets, radically different from the packing of HEL itself. This helix-alignment is also achieved to a good approximation in the 5 donor-acceptor π complexes of HEL with TNB (two different crystal forms), DNBA, TCNQ, and NIPA, with prominent homochiral HEL sheets once again showing up in the latter 3 adducts. We conclude this report with a compilation of implications gleaned from our results, which we deem are of some relevance to stimulate further work.

1) The stability and insolubility of the $(TMA)_2 \cdot COR$ complex may be of use in recovering COR from coal tar pitch or other industrial PAH mixtures, as well as for purification of COR. At present, COR is a rather expensive commodity (about $ 160 per gram of 97% pure material) and no simple synthesis is available.

2) We have produced evidence in this work that in the disordered crystals of $(TMA)_2 \cdot COR$, the orientation of the COR molecules in the hexagonal TMA host cavities should correspond to that shown in *Fig. 1, a*. Further and rather direct support could possibly come from scanning probe microscopy (scanning-tunneling microscopy, STM; atomic force microscopy, AFM), in view of the rather large dimensions of the supramolecular architecture, a true nanostructure. Good surfaces should be straightforward to bring about, considering the extremely facile cleavage of the crystals perpendicular to the hexagonal needle axis. Furthermore, the creation of monolayers or multi-layered *Langmuir-Blodgett* films on suitable substrates may possibly also be conceived, although the adduct's generally low solubility is counter-productive here.

3) It appears probable that [18]annulene (ANN) forms a complex with TMA of composition $(TMA)_2 \cdot ANN$, whose structure is expected to be entirely analogous to that of $(TMA)_2 \cdot COR$, including a likely stacking disorder of the super-graphite sheets. Should these envisaged sheets, however, for some reason stack in an ordered fashion, the possibility of a precision measurement of the structure of ANN would open up. This would be a welcome opportunity to confirm the delocalized, aromatic nature of this theoretically important hydrocarbon. In the crystals of ANN itself, the molecule is partially orientationally disordered hampering truly incisive conclusions [15]. In the presumptive complex $(TMA)_2 \cdot ANN$, orientational disorder of the 18-membered ring is unlikely due to the good C–H···O contacts (analogous to *Fig. 1, a*) by which ANN is expected to be suspended in the hexagonal TMA host chambers.

4) The crystallization properties of $(TMA)_2 \cdot HEL$ are excellent, and large single crystals of good quality are easily obtained, which take the shape of thick pseudo-hexagonal, basalt-like prisms. They may be readily cleaved perpendicular to the pseudo-hexagonal axis. The smooth surfaces thus exposed are expected to consist of domains built up of super-graphite sheets (*Fig. 3*) with homochiral, helix-aligned HEL

molecules anchored in the hexagonal TMA host chambers. Neighboring surface domains formed by adjacent super-graphite sheets would then involve HEL molecules of opposite chirality, but again all homochiral, of course. The intriguing possibility would arise to directly observe the HEL chiralities in the surface domains by scanning-probe microscopic techniques. Clearly, these surfaces would also be attractive targets as regards their chiroptic and non-linear optical (NLO) properties (see below). Multi-layered *Langmuir-Blodgett* films of $(TMA)_2 \cdot HEL$ could also be envisaged with the exposed top layer consisting of a single super-graphite sheet with homochiral, helix-aligned HEL molecules. As to the creation of $(TMA)_2 \cdot HEL$ monolayers, see below.

5) Evidently, the donor-acceptor complexes $HEL \cdot DNBA$ and $HEL \cdot TCNQ$ are also of interest concerning the exposure of surfaces densely packed with homochiral, helix-aligned HEL molecules (*Figs. 7* and *8*). However, due to lack of helicene material and ensuing paucity of crystals, unfortunately no information on their cleavage behavior could be obtained as yet.

6) The layered crystal architectures of $(TMA)_2 \cdot HEL$, $HEL \cdot DNBA$, $HEL \cdot TCNQ$, and $(NIPA)_2 \cdot HEL$ with their sheets of homochiral, helix-aligned HEL molecules, whose chirality changes from sheet to sheet, are of further interest in conjunction with optical-frequency conversion. These structural characteristics of our crystalline HEL complexes are exactly those required for so-called quasi-phase-matched structures, which are relevant in this NLO context [16].

7) Within this study, we have dealt with racemic HEL complexes throughout, and the implications of our results pondered upon thus far, all refer to racemic materials. Perhaps the most important conclusion to be drawn from our study concerns its extension to molecular complexes of non-racemic, enantiomerically pure HEL. Whether non-racemic, optically active HEL forms a crystalline complex with TMA consisting of stacked super-graphite sheets like in racemic $(TMA)_2 \cdot HEL$, is difficult to predict. Doubts may be raised since our results with racemic HEL indicate that the stacking of super-graphite sheets with alternating HEL chiralities appears to be more favorable than piling up sheets with like chiralities. This follows simply from the fact that no enantiomer resolution was observed on crystallizing the $(TMA)_2 \cdot HEL$ complex with racemic HEL in several experiments. Space-filling mechanical models are difficult to manipulate because of the dimension of the problem, and ultimately experiment or perhaps a detailed computer-assisted modeling analysis will have to decide whether or not a satisfactory stacking of super-graphite sheets with like helicene chiralities may be attained without leaving open substantial empty spaces. On the other hand, there appears to be no obvious reason to doubt the feasability of creating donor-acceptor π complexes of optically active HEL with helix-aligned helicene molecules. Layered, helix-aligned architectures similar to those observed in the racemic complexes $HEL \cdot DNBA$ and $HEL \cdot TCNQ$ should also be within reach. Indeed, there appears to be a reasonable chance that optically active HEL, too, forms crystalline complexes with DNBA and TCNQ involving these structural features. Whether optically active HEL will engage in a stable complex with NIPA, is more difficult to assess, however, for related reasons as in the case of a TMA adduct with non-racemic HEL (see above). Clearly, the general diamondoid, crossed fence-type structure of *Figs. 9, e – g*, cannot be upheld if exclusively HEL molecules of one particular chirality are available for

binding to NIPA. Work is in progress in our laboratory to address these intriguing questions and prospects of crystal engineering.

8) Complexes of optically active HEL with helix-aligned, layered structures would again be very interesting targets for scanning-probe microscopy experiments, and the opportunity opens up to directly observe the absolute HEL chirality and to match it with that derived by other means, *e.g.*, by X-ray anomalous scattering or chemical correlation. Whether multi-layered films of nonracemic $(TMA)_2 \cdot$ HEL can be made, is questionable, as is the existence of such a crystalline complex altogether (see above). However, optically active $(TMA)_2 \cdot$ HEL monolayers with helix-aligned HEL molecules corresponding to the homochiral super-graphite sheets of racemic $(TMA)_2 \cdot$ HEL appear feasible. They could possibly even be created from racemic HEL, provided the homochiral $(TMA)_2 \cdot$ HEL sheet happens to be energetically more favorable than heterochiral variants. This would require that the mode of puckering of the H-bonded TMA honeycomb sheets supporting the uptake of the HEL guest molecules is energetically cheapest for the homochiral case (see *Sect. 2*). However, the chirality sense of the monolayer could obviously not be controlled when combining racemic HEL with TMA.

9) An important material-scientific aspect of crystalline, helix-aligned complexes of non-racemic HEL concerns their expected extreme chiroptic and non-linear optical (NLO) properties, *i.e.*, very high specific rotations and second-order NLO susceptibilities in the solid state, for example. Following a different strategy, this has been demonstrated recently in impressive work on optically active, covalent HEL derivatives equipped with long alkyl side-chains. These extended substituents support the formation of columnar aggregates with helix-aligned, homochiral HEL moieties. Strong enhancement of chiroptic and NLO properties was observed [16][17]. Clearly, these observations on molecular, covalent HEL derivatives should carry over to the crystalline complexes of optically active HEL envisaged here, which may be viewed as corresponding supramolecular derivatives. Quite generally, the molecular and/or supramolecular engineering of helix-aligned chiral materials would appear to map out an important area for rewarding future work.

10) It goes almost without saying that the present work should be extended to other helicenes, that is carbohelicenes and heterohelicenes alike, as well as other helically shaped molecules, both optically active and racemic. Of particular interest are higher helicenes, and it would, for example, be interesting to see whether higher carbohelicenes composed of more than 6 fused benzene rings still show a propensity to form complexes with TMA. Obviously, within the hexagonal H-bonded TMA honeycomb sheets, this is by no means guaranteed, considering the increasingly deviating molecular thicknesses of host and guest, and ensuing special stacking requirements. Donor-acceptor π complexes of higher helicenes would, on the other hand, not appear to be subjected to supramolecular constraints of this kind. For sobering, however, it is finally only fair to say that supramolecular work with helicenes will generally not be a particularly comfortable occupation, since it will require a substantial preparative chemical effort, including enantiomer separation, as these materials are usually not accessible *via* simple and standard synthetic routes.

Experimental Part

Crystallizations and Crystal-Structure Analyses. Commercial samples were used throughout for the crystallizations. Only a small sample of racemic HEL was available, and the respective experiments had to be performed with small amounts, *i.e.* a few milligrams, at most, of (recovered) material. Fortunately, all the 6 HEL adducts reported crystallize well. The crystallographic X-ray measurements were performed on a *Nonius*-4-circle diffractometer equipped with a *CCD* area counter using Mo radiation (λ 0.71073 Å). The structures were solved and refined with the programmes SHELXS97 and SHELXL97, respectively. Crystal and X-ray anal. data of the HEL adducts are collected in the *Table*[3]). Further relevant details, especially crystallization conditions, are given below. The COR complexes are included, although they do not appear in the *Table*, and no further quantitative information is reported or deposited. The crystallographic properties of the disordered adduct $(TMA)_2 \cdot COR$ and its crystal chemistry, being of key importance to the present study, are only detailed in the *General Part* (*Sect. 2*), as well as brief qualitative respective accounts of the other COR complexes.

Benzene-1,3,5-tricarboxylic Acid Compound with Coronene (2:1) ($(TMA)_2 \cdot COR$). Crystals were obtained by suitable diffusion procedures as reported in *Sect. 2*. Their structure could not be elucidated directly, probably due to disorder effects. The structure of this adduct may nevertheless be largely guessed by more indirect evidence (see *Sect. 2*).

Benzene-1,3,5-tricarboxylic Acid Compound with (±)-Phenanthro[3,4-c]phenanthrene (2:1) ($(TMA)_2 \cdot HEL$). Excellent large crystals were obtained from a mixture of CS_2, AcOH, and EtOH. They grew in bunches of pale-yellow, thick 6-sided prisms reminiscent of basalt pillars. Crystal size: *ca.* $0.5 \times 0.4 \times 0.4$ mm. Data sets were recorded at r.t. and at 105 K (*Table*), and the results of both measurements are deposited[3]).

(±)-Phenanthro[3,4-c]phenanthrene Compound with 1,3,5-Trinitrobenzene (1:1) ($HEL \cdot TNB$). Dark-yellow crystals were obtained from 1,2-dichloroethane under ambient conditions. They appeared as parallelepipedic plates, and two separate forms could be identified differing in obliqueness. The X-ray analysis established the different crystallography of the two concurrently grown crystal species, one belonging to the triclinic, the other to the monoclinic system. Crystal sizes: *ca.* $0.4 \times 0.4 \times 0.15$ mm.

(±)-Phenanthro[3,4-c]phenanthrene Compound with 3,5-Dinitrobenzoic Acid (1:1) ($HEL \cdot DNBA$). Small, deep-yellow crystal plates were grown from 1,2-dichloroethane. Crystal size: *ca.* $0.2 \times 0.2 \times 0.1$ mm.

(±)-Phenanthro[3,4-c]phenanthrene Compound with 2,2′-(Cyclohexa-2,5-diene-1,4-diylidene)bis[propanedinitrile] (1:1) $HEL \cdot TCNQ$. The complex was crystallized from 1,2-dichloroethane: bluish-black crystal laths. Crystal size: $0.4 \times 0.3 \times 0.15$ mm.

5-Nitrobenzene-1,3-dicarboxylic Acid Compound with (±)-Phenanthro[3,4-c]phenanthrene (2:1) ($(NIPA)_2 \cdot HEL$). Deep-yellow crystals were precipitated from 1,2-dichloroethane and a small amount of EtOH, just about sufficient to keep the diacid in solution. The crystals grew in flower-like groups of wedge-shaped leaflets with curved edges. The thickness of the crystal leaflets reached 0.2 mm and their width up to 1 mm. An NMR spectrum of crystals redissolved in $CD_2Cl_2/(D_6)DMSO$ confirmed the 2:1 stoichiometry of the complex within experimental error. A crystal specimen trimmed to $0.4 \times 0.2 \times 0.2$ mm was used for the X-ray measurement at 105 K. A number of doubled reflections showed up during data processing, the intensities of which were integrated over both constituent spots. The crystal structure of $(NIPA)_2 \cdot HEL$ could be smoothly solved by direct methods in space group *Cc*. The higher centrosymmetric crystal symmetry *C*2/*c* is roughly approximated, but no structure solution could be obtained in this space group. Moreover, trial refinements in *C*2/*c* with symmetry-averaged starting structures proved highly unsatisfactory with soaring agreement factors and were quickly abandoned. While the 6 independent NIPA molecules and 2 of the 3 independent HEL molecules showed moderate temp. motion, the remaining third independent HEL molecule assumed high anisotropic temp. motion parameters in the refinement, coupled with a rather distorted molecular geometry. It was ultimately optimized as a rigid body with two split half-weight orientations, as suggested by the shapes of the temperature-factor ellipsoids. Expectedly, both orientations are related by rotation around an axis roughly parallel to the helix axis (*Fig. 9, b*). The rigid-body geometry of this twofold orientationally disordered HEL molecule was taken over from $HEL \cdot TCNQ$.

---

[3]) Crystallographic data (excluding structure factors) for the structures reported in this paper and appearing in the *Table* have been deposited with the *Cambridge Crystallographic Data Centre* as deposition No. CCDC-158116 – CCDC-158123. Copies of the data can be obtained, free of charge, on application to the CCDC, 12 Union Road, Cambridge CB2 1EZ, UK (fax: +44(1223)336033; e-mail : deposit@ccdc.cam.ac.uk).

Phenanthrene Compound with 5-Nitrobenzene-1,3-dicarboxylic Acid (1:1) (PHEN·NIPA). Bundles of needle-shaped crystals with rhomb-shaped cross-section were obtained quantitatively from aqueous EtOH. The color of the bulk crystalline material was lemon-yellow while individual needle specimens of X-ray size appeared paler yellow in transmittent light. The crystal needles could be cleaved with relative ease approximately perpendicular to the needle axis, but less readily than $(TMA)_2$·HEL and much less facile than $(TMA)_2$·COR.

Coronene Compound with 1,3,5-Trinitrobenzene (1:1) (COR·TNB). Long, brownish-red needles were obtained by diffusion after placing the following 3 layers of miscible liquids on top of each other in a test tube: *i*) CS_2 soln. of COR, *ii*) AcOH/1,2-dichloroethane 1:1, and *iii*) AcOH soln. of TNB. Crystal size: *ca.* $0.4 \times 0.4 \times 0.3$ mm. Cell data: $a = 7.0342(4)$, $b = 16.0601(9)$, $c = 19.8594(10)$ Å, $\beta = 93.021(3)^\circ$, space group $P2_1/n$, $Z = 4$. The refinement of the structure showed the COR molecules to be orientationally disordered with two preferred and roughly equally populated orientations related by rotation around the 6-fold molecular axis of COR.

Coronene Compound with 3,5-Dinitrobenzoic Acid (1:1) (COR·DNBA). Orange-yellow needles of substantial size were grown by diffusion according to the same recipe as for the COR·TNB complex. Crystal size similar to that of COR·TNB. Cell data: $a = 16.8624(5)$, $b = 6.9307(3)$, $c = 19.6684(6)$ Å; $\beta = 92.237(2)^\circ$; space group $P2_1/c$; $Z = 4$. The COR molecules in this adduct showed orientational disorder, similar to that found in COR·TNB.

5-Nitrobenzene-1,3-dicarboxylic Acid Compound with Coronene (2:1) ($(NIPA)_2$·COR). Rosette-like groups of thick orange-red crystal leaflets with curved edges were grown by triple-layer diffusion in a slim, tilted beaker: A CS_2 soln. of COR was covered by an AcOH layer, which in turn was topped by an EtOH soln. of NIPA. A large excess (*ca.* 10-fold) of NIPA was used. The crystals diffracted X-rays relatively well, although reflections with irregular shapes and streaks were spotted. No reliable cell dimensions or even structural information could be derived from these crystals, however, whose 2:1 composition was established by an NMR spectrum (CD_2Cl_2/(D_6)DMSO). Presumably, the crystals of $(NIPA)_2$·COR are subject to severe disorder phenomena.

REFERENCES

[1] a) D. J. Duchamp, R. E. Marsh, *Acta Crystallogr., Sect. B* **1969**, *25*, 5; b) F. H. Herbstein, in 'Comprehensive Supramolecular Chemistry', Eds. J. L. Atwood, J. E. D. Davies, D. D. MacNicol, and F. Vögtle, Pergamon, 1996, Vol. 6, Chapt. 3, p. 61; c) S. V. Kolotuchin, P. A. Thiessen, E. E. Fenlon, S. R. Wilson, C. J. Loweth, S. C. Zimmerman, *Chem.–Eur. J.* **1999**, *5*, 2537.

[2] a) F. H. Herbstein, M. Kapon, S. Wasserman, *Acta Crystallogr., Sect. B* **1978**, *34*, 1613; b) F. H. Herbstein, R. E. Marsh, *Acta Crystallogr., Sect. B* **1977**, *33*, 2358.

[3] J. M. Robertson, J. G. White, *J. Chem. Soc.* **1945**, 607; J. K. Fawcett, J. Trotter, *Proc. R. Soc. London, Ser. A* **1965**, *289*, 366; T. M. Krygowski, M. Cyranski, A. Ciesielski, B. Swirska, P. Leszczynski, *J. Chem. Inf. Comput. Sci.* **1996**, *36*, 1135.

[4] G. R. Desiraju, T. Steiner, 'The Weak Hydrogen Bond', Oxford Univ. Press, Oxford, 1999.

[5] W. H. Zachariasen, *Acta Crystallogr.* **1954**, *7*, 305; B. M. Craven, T. M. Sabine, *Acta Crystallogr.* **1966**, *20*, 214.

[6] C. de Rango, G. Tsoucaris, J. P. Declercq, G. Germain, J. P. Putzeys, *Cryst. Struct. Commun.* **1973**, *2*, 189.

[7] O. Ermer, S. Lifson, *J. Am. Chem. Soc.* **1973**, *95*, 4121.

[8] D. E. Koshland, *Proc. Natl. Acad. Sci. U.S.A.* **1958**, *44*, 98.

[9] B. S. Green, M. Knossow, *Science (Washington, D.C.)* **1981**, *214*, 795; S. Ramdas, J. M. Thomas, M. E. Jordan, C. J. Eckhardt, *J. Phys. Chem.* **1981**, *85*, 2421.

[10] a) O. Ermer, A. Eling, *Angew. Chem., Int. Ed.* **1988**, *27*, 829; b) O. Ermer, L. Lindenberg, *Chem. Ber.* **1990**, *123*, 1111.

[11] A. Domenicano, G. Schultz, I. Hargittai, M. Colapietro, G. Portalone, P. George, C. W. Bock, *Struct. Chem.* **1990**, *1*, 107.

[12] M. I. Kay, Y. Okaya, D. E. Cox, *Acta Crystallogr., Sect. B* **1971**, *27*, 26.

[13] O. Ermer, S. A. Mason, *J. Chem. Soc., Chem. Commun.* **1983**, *53*; O. Ermer, S. A. Mason, F. A. L. Anet, S. S. Miura, *J. Am. Chem. Soc.* **1985**, *107*, 2330.

[14] E. Fischer, *Ber. Dtsch. Chem. Ges.* **1894**, *27*, 2985.

[15] J. Bregman, F. L. Hirshfeld, D. Rabinovich, G. M. J. Schmidt, *Acta Crystallogr.* **1965**, *19*, 227; F. L. Hirshfeld, D. Rabinovich, *Acta Crystallogr.* **1965**, *19*, 235; S. Gorter, E. Rutten-Keulemans, M. Krever, C. Romers, D. W. J. Cruickshank, *Acta Crystallogr., Sect. B* **1995**, *51*, 1036.
[16] T. Verbiest, S. van Elshocht, M. Kauranen, L. Hellemans, J. Snauwaert, C. Nuckolls, T. J. Katz, A. Persoons, *Science (Washington, D.C.)* **1998**, *282*, 913.
[17] C. Nuckolls, T. J. Katz, L. Castellanos, *J. Am. Chem. Soc.* **1996**, *118*, 3767; A. J. Lovinger, C. Nuckolls, T. J. Katz, *J. Am. Chem. Soc.* **1998**, *120*, 264.

Received February 23, 2001